

# 1 Mid-Holocene Climate Change over China: Model-Data Discrepancy

2 Yating Lin <sup>1,2,4</sup>, Gilles Ramstein <sup>2</sup>, Haibin Wu <sup>1,3,4</sup>, Raj Rani <sup>2</sup>, Pascale Braconnot <sup>2</sup>,

3 Masa Kageyama <sup>2</sup>, Qin Li <sup>1,3</sup>, Yunli Luo <sup>5</sup>, Ran Zhang <sup>6</sup> and Zhengtang Guo <sup>1,3,4</sup>

4 1. Key Laboratory of Cenozoic Geology and Environment, Institute of Geology and  
5 Geophysics, Chinese Academy of Sciences, Beijing 100029, China

6 2. Laboratoire des Sciences du Climat et de l'Environnement, LSCE/IPSL,  
7 CEA-CNRS-UVSQ, Université Paris-Saclay, Gif-sur-Yvette 91191, France

8 3. CAS Center for Excellence in Life and Paleoenvironment, Beijing, 100044, China

9 4. University of Chinese Academy of Sciences, Beijing 100049, China

10 5. Institute of Botany, Chinese Academy of Sciences, Beijing 100093, China

11 6. Institute of Atmospheric Physics, Chinese Academy of Sciences, Beijing 100029, China

## 12 **Abstract:**

13 The mid-Holocene period (MH) has long been an ideal target for the validation of Global  
14 Circulation Model (GCM) results against reconstructions gathered in global datasets. These  
15 studies aim to test the GCM sensitivity mainly to the seasonal changes induced by the orbital  
16 parameters (precession). Despite widespread agreement between model results and data on the  
17 MH climate, some important differences still exist. There is no consensus on the continental  
18 size of the MH thermal climate response, which makes regional quantitative reconstruction  
19 critical to obtain a comprehensive understanding of the MH climate patterns. Here, we compare  
20 the annual and seasonal outputs from the most recent Paleoclimate Modelling Intercomparison  
21 Projects Phase 3 (PMIP3) models with an updated synthesis of climate reconstruction over  
22 China, including, for the first time, a seasonal cycle of temperature and precipitation. Our  
23 results indicate that the main discrepancies between model and data for the MH climate are the  
24 annual and winter mean temperature. A warmer-than-present climate condition is derived from  
25 pollen data for both annual mean temperature (~0.7 K on average) and winter mean temperature

26 (~1 K on average), while most of the models provide both colder-than-present annual and  
27 winter mean temperature and a relatively warmer summer, showing linear response driven by  
28 the seasonal forcing. By conducting simulations in BIOME4 and CESM, we show that the  
29 surface processes are the key factors drawing the uncertainties between models and data. These  
30 results pinpoint the crucial importance of including the non-linear responses of the surface  
31 water and energy balance to vegetation changes.

32

33 *Keywords:* PMIP3    Pollen data    Inverse Vegetation Model    Seasonal climate change

34

35

## 36 **1. Introduction**

37        Much attention of paleoclimate study has been focused on the current interglacial (the  
38 Holocene), especially the mid-Holocene (MH,  $6\pm 0.5$  ka). The major difference in the  
39 experimental configuration between the MH and pre-Industrial (PI) arises from the orbital  
40 parameters which brings about an increase in the amplitude of the seasonal cycle of insolation  
41 of the Northern Hemisphere and a decrease in the Southern Hemisphere (Berger, 1978). Thus,  
42 the MH provides an excellent case study on which to base an evaluation of the climate response  
43 to changes in the distribution of insolation. Great efforts are devoted by the modeling  
44 community to the design of the MH common experiments using similar boundary conditions  
45 (Joussaume and Taylor., 1995; Harrison et al., 2002; Braconnot et al., 2007a, b). In addition,  
46 much work has been done to reconstruct the paleoclimate change based on different proxies at  
47 global and continental scale (Guiot et al., 1993; Kohfeld and Harrison, 2000; Prentice et al.,  
48 2000; Bartlein et al., 2011). The greatest progress in understanding the MH climate change and

49 variability has consistently been made by comparing large-scale analyses of data with  
50 simulations from global climate models (Joussaume et al., 1999; Liu et al., 2004; Harrison et al.,  
51 2014).

52 However, the source of discrepancies between model and data is still an open and stimulating  
53 question. Two types of inconsistencies have been identified: 1) where the model and data show  
54 opposite signs, for instance, paleoclimate evidence from data-records indicates an increase of  
55 about 0.5 K in global annual mean temperature during the MH compared with PI (Shakun et al.,  
56 2012; Marcott et al., 2013), while there is a cooling trend in model simulations (Liu et al., 2014).  
57 2) where the same trend is displayed by both model and data but with different magnitudes.  
58 Previous studies have shown that while climate models can successfully reproduce the direction  
59 and large-scale patterns of past climate changes, they tend to consistently underestimate the  
60 magnitude of change in the monsoons of the Northern Hemisphere as well as the amount of the  
61 MH precipitation over northern Africa (Braconnot et al., 2012; Harrison et al., 2015). Moreover,  
62 significant spatial variability has been noted in both observations and simulations (Peyron et al.,  
63 2000; Davis et al., 2003; Braconnot et al., 2007a; Wu et al., 2007; Bartlein et al., 2011), which  
64 makes regional quantitative reconstruction (Davis et al., 2003; Mauri et al., 2015) essential to  
65 obtain a comprehensive understanding of the MH climate patterns, and to act as a benchmark to  
66 evaluate climate models (Fischer and Jungclaus, 2011; Harrison et al., 2014;).

67 China offers two advantages in respect to these issues. The sheer expanse of the country  
68 means that the continental response to insolation changes over a large region can be  
69 investigated. Moreover, the quantitative reconstruction of seasonal climate changes during the  
70 MH, based on the new pollen dataset, provides a unique opportunity to compare the seasonal  
71 cycles for models and data. Previous studies indicate that warmer and wetter than present  
72 conditions prevailed over China during the MH and that the magnitude of the annual  
73 temperature increases varied from 2.4-5.8 K spatially, with an annual precipitation increase in

74 the range of 34-267 mm (e.g., Sun et al., 1996; Jiang et al., 2010; Lu et al., 2012; Chen et al.,  
75 2015). However, Jiang et al. (2012) clearly show a mismatch between multi-proxy  
76 reconstructions and model simulations. In terms of climate anomalies (MH-PI), besides the ~1  
77 K increase in summer temperature, 35 out of 36 Paleoclimate Modelling Intercomparison  
78 Projects (PMIP) models reproduce annual (~0.4 K) and winter temperatures (~1.4 K) that are  
79 colder than the baseline, and a drier-than-baseline climate in some western and middle regions  
80 over China is depicted in models (Jiang et al., 2013). Jiang et al. (2012) point out the  
81 model-data discrepancy over China during the MH, but the lack of seasonal reconstructions in  
82 their study limits comparisons with simulations.

83 An important issue raised by Liu et al. (2014) is that the discrepancy at the annual level could  
84 be due to incorrect reconstructions of the seasonal cycle, a key objective in our paper. Moreover,  
85 it has been suggested that the vegetation change can strengthen the temperature response in  
86 high latitudes (O’Ishi et al., 2009; Otto et al., 2009), as well as alter the hydrological conditions  
87 in the tropics (Liu et al., 2007). However, compared to the substantial land cover changes in the  
88 MH derived from pollen datasets (Ni et al., 2010; Yu et al., 2000), the changes in vegetation  
89 have not yet been fully quantified and discussed in PMIP3 (Taylor et al., 2012).

90 In this study, for the reconstruction, we firstly used the quantitative method of biomization to  
91 reconstruct vegetation types during the MH based on a new synthesis of pollen datasets, and  
92 then used the Inverse Vegetation Model (Guiot et al., 2000; Wu et al., 2007) to obtain the  
93 annual, the mean temperature of the warmest month (MTWA) and the mean temperature of the  
94 coldest month (MTCO) climate features over China for the MH. In the case of PMIP3 models,  
95 we present a comprehensive evaluation of the PMIP3 simulations made with state-of-art  
96 climate models using reconstructions of temperature and precipitation. This is the first time that  
97 such progress towards a quantitative seasonal climate comparison for the MH over China has  
98 been made. This point is crucial because the MH PMIP3 experiment is essentially one that

99 looks at the response of the models to changes in the seasonality of insolation, and the attempt  
100 to derive reconstructions of both summer and winter climate to compare with the simulations  
101 will thus be able to answer the question posed by Liu et al. (2014) on the importance of seasonal  
102 reconstruction.

## 103 **2. Data and Methodology**

### 104 **2.1 Data**

105 In this study, we collected 159 pollen records, covering most of China, for the MH period  
106 ( $6000\pm 500$   $^{14}\text{C}$  yr BP) (Fig. 1). Of these, 65 were from the Chinese Quaternary Pollen Database  
107 (CQPD, 2000), three were original datasets obtained in our study, and the others were digitized  
108 from pollen diagrams in published papers with a recalculation of pollen percentages based on  
109 the total number of terrestrial pollen types. These digitized 91 pollen records were selected  
110 according to three criteria: (1) clearly readable pollen diagrams with a reliable chronology with  
111 the minimum of three independent age control points since the LGM; (2) including the pollen  
112 taxa during  $6000\pm 500$   $^{14}\text{C}$  yr BP period with a minimum sampling resolution of 1000 years per  
113 sample; (3) abandon the pollen records if the published paper mentions the influence of human  
114 activity. Based on the digitized pollen assemblages, we use biomization to get the biome scores  
115 and biome types. For age control, different dating methods are utilized in the collected pollen  
116 records, we applied the CalPal 2007 (Weninger et al., 2007) to correct  $^{14}\text{C}$  age into calendar  
117 age so that they can be contrasted with each other. For lacustrine records, if the specific  
118 carbon pool age is mentioned in the literature, the calendar age is corrected after deducting the  
119 carbon pool. Otherwise, the influence of carbon pool is not considered. The age-depth model  
120 for the pollen records was estimated by linear interpolation between adjacent available dates  
121 or by regression. Using ranking schemes from the Cooperative Holocene Mapping Project,  
122 the quality of dating control for the mid-Holocene was assessed by assigning a rank from 1 to

123 7. And 70% of the records used in our study fell into the first and second classes (see Table 1  
124 for detailed information) according to the Webb 1-7 standards (Webb, III T., 1985).  
125 Vegetation type was quantitatively reconstructed using biomization (Prentice et al., 1996),  
126 following the classification of plant functional types (PFTs) and biome assignment in China by  
127 the Members of China Quaternary Pollen Data (CQPD, 2000), which has been widely tested in  
128 surface sediment. The new sites (91 digitized data and three original data) added to our database  
129 improved the spatial coverage of pollen records, especially in the northwest, the Tibetan  
130 Plateau, the Loess Plateau and southern regions, where the data in the previous databases are  
131 very limited.

132 Modern monthly mean climate variables, including temperature, precipitation and  
133 cloudiness (total cloud fraction), applied in this study, have been collected for each modern  
134 pollen site based on the datasets (1951-2001) from 657 meteorological observation stations  
135 over China (China Climate Bureau, China Ground Meteorological Record Monthly Report,  
136 1951-2001). The MH soil properties and characteristics used in inverse vegetation model were  
137 kept the same with PI conditions, which are derived from the digital world soil map produced  
138 by the Food and Agricultural organization (FAO) (FAO, 1995). Atmospheric CO<sub>2</sub>  
139 concentration for the MH was taken from ice core records (EPICA community members 2004),  
140 and was set at 270 ppmv.

141 A 3-layer back-propagation (BP) artificial neural network technique (ANN) was used for  
142 interpolation on each pollen site (Caudill and Butler, 1992). Five input variables (latitude,  
143 longitude, elevation, annual precipitation, annual temperature) and one output variable (biome  
144 scores) have been chosen in ANN for the modern vegetation. The ANN has been calibrated on  
145 the training set, and its performance has been evaluated on the verification set (20%, randomly  
146 extracted from the total sets). After a series of training run, the lowest verification error is  
147 obtained with 5 neurons in the hidden layer after 10000 iterations. The anomalies between past

148 (6 ka) and modern vegetation indices (biome scores) was then interpolated to the  $0.2 \times 0.2^\circ$  grid  
149 resolution by applying the ANN. After that, the modern grid values are added to the values of  
150 the grid of palaeo-anomalies to provide gridded paleo-biome indices. Finally, the biome with  
151 the highest index is attributed to each grid point. This ANN method is more efficient than many  
152 other techniques on condition that the results are validated by independent data sets, and  
153 therefore, it has been widely applied in paleoclimatology (Guiot et al., 1996; Peyron et al.,  
154 1998).

## 155 **2.2 Climate models**

156 PMIP, a long-standing initiative, is a climate-model evaluation project which provides an  
157 efficient mechanism for using global climate models to simulate climate anomalies in the past  
158 periods and to understand the role of climate feedback. In its third phase (PMIP3), the models  
159 were identical to those used in the Climate Modelling Intercomparison Project 5 (CMIP5)  
160 experiments. The experimental set-up for the mid-Holocene simulations in PMIP3 followed the  
161 PMIP protocol (Braconnot et al., 2007a, b, 2012). The main forcing between the MH and PI in  
162 PMIP3 are the orbital configuration and  $\text{CH}_4$  concentration. More precisely, the orbital  
163 configuration in the MH climate has an increased summer insolation and a decreased winter  
164 insolation in the Northern Hemisphere compared to the PI climate (Berger, 1978). Meantime,  
165 the  $\text{CH}_4$  concentration is prescribed at 650 ppbv in the MH, while it is set at 760 ppbv in PI  
166 (Table 2).

167 All 13 models (Table 3) from PMIP3 that have the MH simulation have been included in  
168 our study, including eight ocean-atmosphere (OA) models and five  
169 ocean-atmosphere-vegetation (OAV) models. Means for the last 30 years were calculated from  
170 the archived time-series data on individual model grids for climate variables: near surface  
171 temperature and precipitation flux, which were bi-linearly interpolated to a uniform  $2.5^\circ$  grid,

172 in order to get the bioclimatic variables (e.g. MAT, MAP, MTWM, MTCO, July precipitation)  
173 onto a common grid for comparison with the reconstruction results.

### 174 **2.3 Vegetation model**

175 The vegetation model, BIOME4 is a coupled bio-geography and biogeochemistry model  
176 developed by Kaplan et al. (2003). Monthly mean temperature, precipitation, sunshine  
177 percentage (an inverse measure of cloud area fraction), absolute minimum temperature,  
178 atmospheric CO<sub>2</sub> concentration and subsidiary information about the soil's physical properties  
179 like water retention capacity and percolation rates are the main input variables for the models. It  
180 incorporates 13 plant functional types (PFTs), which have different bioclimatic limits. The  
181 PFTs are based on physiological attributes and bioclimatic tolerance limits such as heat,  
182 moisture and chilling requirements and resistance of plants to cold. These limits determine the  
183 areas where the PFTs could grow in a given climate. A viable combination of these PFTs  
184 defines a particular biome among 28 potential options. These 28 biomes can be further  
185 classified into 8 megabiomes (Table S1). BIOME4 has been widely utilized to analyze the past,  
186 present and potential future vegetation patterns (e.g. Bigelow et al., 2003; Diffenbaugh et al.,  
187 2003; Song et al., 2005). In this study, we conducted 13 PI and the MH biome simulations using  
188 PIMP3 climate fields (temperature, precipitation and sunshine) as inputs. The climate fields,  
189 obtained from PMIP3, are the monthly mean data of the last 30 model years.

### 190 **2.4 Statistics and interpolation for vegetation distribution**

191 To quantify the differences between simulated (by the climate-model output) and  
192 reconstructed (from pollen) between megabiomes, a map-based statistic (point-to-point  
193 comparison with observations) called  $\Delta V$  (Sykes et al., 1999; Ni et al., 2000) was applied to  
194 our study.  $\Delta V$  is based on the relative abundance of different plant life forms (e.g. trees, grass,  
195 bare ground) and a series of attributes (e. g. evergreen, needle-leaf, tropical, boreal) for each



196 vegetation class. The definitions and attributes of each plant form follow naturally from the  
197 BIOME4 structure and the vegetation attribute values in the  $\Delta V$  computation were defined for  
198 BIOME4 in the same way as for BIOME1 (Sykes et al., 1999). The abundance and attribute  
199 values are given in Table 4 and Table 5, which describe the typical floristic composition of the  
200 biomes. Weighting the attributes is subjective because there is no obvious theoretical basis for  
201 assigning relative significance. Transitions between highly dissimilar megabiomes have a  
202 weighting of close to 1, whereas transitions between less dissimilar megabiomes are assigned  
203 smaller values. The overall dissimilarity between model and data megabiome maps was  
204 calculated by averaging the  $\Delta V$  for the grids with pollen data, while the value was set at 0 for  
205 any grid without data.  $\Delta V$  values  $< 0.15$  can be considered to point to very good agreement  
206 between simulated and actual distributions, 0.15-0.30 is good, 0.30-0.45 is fair, 0.45-0.60 is  
207 poor, and  $> 0.80$  is very poor (adjusted from Zhang et al., 2010). For spatial pattern comparison,  
208 we compared the simulated vegetation distribution from BIOME4 from each model with the  
209 interpolated pattern of reconstruction.

## 210 **2.5 Inverse vegetation model**

211 Inverse Vegetation Model (Guiot et al., 2000; Wu et al., 2007), highly dependent on the  
212 BIOME4 model, is applied to our reconstruction. The key concept of this model can be  
213 summarized in two points: firstly, a set of transfer functions able to transform the model output  
214 into values directly comparable with pollen data is defined. There is not full compatibility  
215 between the biome typology of BIOME4 and the biome typology of pollen data. A transfer  
216 matrix (Table S2) was defined in our study where each BIOME4 vegetation type is assigned a  
217 vector of values, one of each pollen vegetation type, ranging from 0 (representing an  
218 incompatibility between BIOME4 type and pollen biome type) to 15 (corresponding to a  
219 maximum compatibility). Secondly, using an iterative approach, a representative set of climate  
220 scenarios compatible with the vegetation records is identified among the climate space,

221 constructed by systematically perturbing the input variables (e.g.  $\Delta T$ ,  $\Delta P$ ) of the model (Table  
222 S3).

223 Inverse Vegetation Model (IVM) provides a possibility, for the first time, to reconstruct both  
224 annual and seasonal climates for the MH over China. Moreover, it offers a way to consider the  
225 impact of CO<sub>2</sub> concentration on competition between PFTs as well as on the relative abundance  
226 of taxa, and thus make reconstruction from pollen records more reliable. More detailed  
227 information about IVM can be found in Wu et al. (2007).

228 We applied the inverse model to modern pollen samples to validate the approach by  
229 reconstructing the modern climate at each site and comparing it with the observed values. The  
230 high correlation coefficients ( $R=0.75-0.95$ ), intercepts close to 0 (except for the mean  
231 temperature of the warmest month), and slopes close to 1 (except for the July precipitation)  
232 demonstrated that the inversion method worked well for most variables in China (see Table 6).

### 233 **3. Results**

#### 234 **3.1 Comparison of annual and seasonal climate changes at the MH**

235 In this study, we collected 159 pollen records, broadly covering the whole of China (Fig. 1).  
236 To check the reliability of the collected data, we first categorized our pollen records into  
237 megabiomes in line with the standard tables developed for the BIOME6000 (Table S1), and  
238 compared them with the BIOME6000 dataset (Fig.2). The match between collected data and  
239 the BIOME6000 is more than 90% (145 out of 159 sites) for both the MH and PI.

240 Based on pollen records, the spatial pattern of climate changes over China during the MH,  
241 deduced from IVM, are presented in Fig. 3 (left panel, points), alongside the results from  
242 PMIP3 models (shaded in Fig. 3). For temperature, a warmer-than-present annual climate  
243 condition ( $\sim 0.7$  K on average) is derived from pollen data (the points in Fig. 3a), with the

244 largest increase occurring in the northeast (3-5 K) and a decrease in the northwest and on  
245 Tibetan Plateau. On the other hand, the results from a multi-model ensemble (MME) indicate a  
246 colder annual temperature generally ( $\sim -0.4$  K on average), with significant cooling in the south  
247 and slight warming in the northeast (shaded in Fig. 3a). Of the 13 models, 11 simulate a cooler  
248 annual temperature compared with PI as MME. However, two models (HadGEM2-ES and  
249 CNRM-CM5) present the same warmer condition as was found in the reconstruction (Fig. 3d).  
250 Compared to the reconstruction, the annual mean temperature during the MH is largely  
251 underestimated by most PMIP3 models, which depict an anomaly ranging from  $\sim -1$  to  $\sim -0.5$  K.  
252 Concerning seasonal change, during the MH, MTWA from the data is  $\sim 0.5$  K higher than PI,  
253 with the largest increase in the northeast and a decrease in the northwest. From model outputs,  
254 an average increase of  $\sim 1.2$  K is reproduced by MME, with a more pronounced warming at high  
255 latitudes which is consistent with the insolation change (Berger, 1978). Fig. 3e shows that all 13  
256 models reproduce the same warmer summer temperatures as the data, and that HadGEM2-ES  
257 and CNRM-CM5, reproduce the largest increases among the models. Although the warmer  
258 MTWA is consistent between the models and data, there is a discrepancy between them on  
259 MTCO. In Fig. 3c, the data show an overall increase of  $\sim 1$  K, with the largest increase occurring  
260 in the northeast and a decrease of opposite magnitude on the Tibetan Plateau. Inversely, MME  
261 reproduces a decreased MTCO with an average amplitude of  $\sim -1.3$  K, the coolest areas being  
262 the southeast, the Loess Plateau and the northwest. Similarly to the MME, all 13 models  
263 simulate a colder-than-present climate with amplitudes ranging from  $\sim -2.0$  K (CCSM4 and  
264 FGOALS-g2) to  $\sim -0.7$  K (HadGEM2-ES and CNRM-CM5).

265 Concerning annual change in precipitation, the reconstruction shows wetter conditions  
266 during the MH across almost the whole of China with the exception of part of the northwest.  
267 The southeast presents the largest increase in annual precipitation. All but 2 models  
268 (MIROC-ESM and FGOALS-g2) depict wetter conditions with an amplitude of  $\sim 10$  mm to  $\sim 50$

269 mm. The reconstruction and MME results also indicate an increased annual precipitation during  
270 MH (Fig.4a), with a much larger magnitude visible in the reconstruction (~30 mm, ~230 mm  
271 respectively). The main discrepancy in annual precipitation between simulations and  
272 reconstruction occurs in the northeast, which is depicted as drier by the models and wetter by  
273 the data. With regard to seasonal change, the reconstruction shows an overall increase in July  
274 rainfall (~50 mm on average), with a decrease in the northwestern regions and East Monsoon  
275 region at Yangtze River valley. In line with the reconstruction, the MME also shows an overall  
276 increase in rainfall (~7 mm on average), with a decrease in the northwest for July (Fig.4b).  
277 Notably, a much larger increase is simulated for the south and the Tibetan Plateau by the  
278 models, while the opposite pattern emerges along the eastern margin from both models and data.  
279 For January precipitation, the reconstruction shows an overall increase in most region (~15  
280 mm), except for the northwestern region, while MME indicates a slight decrease (~3 mm on  
281 average). More detailed information about the geographic distribution of simulated temperature  
282 and precipitation for each model can be found in Fig. S1-S6.

283 Table S4 provides the biome score from IVM for pollen data collected from published papers.  
284 The reconstructed climate change derived from IVM at each pollen site can be found in Table  
285 S5, in which the columns show the median and the 90% interval (5th to 95th percentage) for  
286 feasible climate values produced with the IVM approach. The simulated values for each of the  
287 climate variables as shown in the boxplots (Figure 3 and Figure 4) are given in the Table S6  
288 and Table S7.

289

### 290 **3.2 Comparison of vegetation change at the MH**

291 The use of the PMIP3 database is clearly limited by the different vegetation inputs among the  
292 models for the MH period (Table S8). Only HadGEM2-ES and HadGEM2-CC use a dynamic  
293 vegetation for the MH, and the other 11 models are prescribed to PI with or without interactive

294 LAI, which would introduce a bias to the role of vegetation-atmosphere interaction in the MH  
295 climates. To evaluate the model results against the reconstruction for the MH vegetation, we  
296 conducted 13 biome simulations in BIOME4 using PIMP3 climate fields, and the megabiome  
297 distribution for each model during the MH is displayed in Fig. 5 (see Fig. S7 for PI vegetation  
298 comparison). To quantify the model-data dissimilarity between megabiomes, a map-based  
299 statistic called  $\Delta V$  (Sykes et al., 1999; Ni et al., 2000) was applied here (detailed information is  
300 in the methodology section).

301 Fig. S8 shows the dissimilarity between simulations and observations for megabiomes  
302 during the MH, with the overall values for  $\Delta V$  ranging from 0.43 (HadGEM2-ES) to 0.55  
303 (IPSL-CM5A-LR). According to the classification of  $\Delta V$  (see in the methodology section) for  
304 the 13 models, 12 (all except HadGEM2-ES) showed poor agreement with the observed  
305 vegetation distribution. Most models poorly simulate the desert, grassland and tropical forest  
306 areas for both periods, but perform better for warm mixed forest, tundra and temperate forest.  
307 However, this statistic is based on a point-to-point comparison and so the  $\Delta V$  calculated here  
308 cannot represent an estimation of full vegetation simulation due to the uneven distribution of  
309 pollen data and the potentially huge difference in area of each megabiome. For instance, tundra  
310 in our data for PI is represented by only 4 points, which counts for a small contribution to the  
311  $\Delta V$  since we averaged it over a total of 159 points, but this calculation could induce a  
312 significant bias if these 4 points cover a large area of China.

313 So, we used the biome scores based on the artificial neural network technique as described by  
314 Guiot et al. (1996) for interpolation (the plots in red rectangle in Fig. 5), and compared the  
315 simulated vegetation distribution from BIOME4 for each model with the interpolated pattern.  
316 During the MH, most models are able to capture the tundra on the Tibetan Plateau as well as the  
317 combination of warm mixed forest and temperate forest in the southeast. However, all models  
318 fail to simulate or underestimate the desert area in the northwest compared to reconstructed data.

319 The main model-data inconsistency in the MH vegetation distribution occurs in the northeast,  
320 where data show a mix of grassland and temperate forest, and the models show a mix of  
321 grassland and boreal forest.

322 The area statistic carried out for simulated vegetation changes (Fig. 6) reveals that the main  
323 difference during the MH, compared with PI, is that grassland replaced boreal forest in large  
324 tracts of the northeast (Fig. 5, Fig. S7). No other significant difference in vegetation distribution  
325 between the two periods was derived from models. Unlike in models, three main changes in  
326 megabiomes during the MH are depicted by the data. Firstly, the megabiomes converted from  
327 grassland to temperate forest in the northeast. Secondly, a large area of temperate forest was  
328 replaced in the southeast by a northward expansion of warm mixed forest. Thirdly, in the  
329 northwest and at the northern margin of the Tibetan Plateau, part of the desert area changed into  
330 grassland. However, none of the models succeed in capturing these features, especially the  
331 transition from grassland into forest in the northeast during the MH. Therefore, this failure to  
332 capture vegetation changes between the two periods will lead to a cumulating inconsistency in  
333 the model-data comparison for climate anomalies because of the vegetation-climate feedbacks.

## 334 **4. Discussion**

### 335 **4.1 Validation and uncertainties for reconstruction**

336 To investigate the discrepancy between model-data for the MH climate change over China,  
337 the reliability of our reconstruction should be firstly considered. For the cross-proxy validation,  
338 we compared our reconstruction with previous studies concerning the MH climate change over  
339 China based on multiple proxies (including pollen, lake core, palaeosol, ice core, peat and  
340 stalagmite), the related references and detailed information are listed in Supplementary  
341 Information (Table S9 and Table S10). In comparison with PI condition, most reconstructions  
342 reproduced warmer and wetter annual condition during the MH (Fig. 7), same as our study. In

343 other words, this discrepancy between model-data for climate change over China during the  
344 MH is common and robust in reconstructions derived from different proxies. Our study just  
345 reinforces the picture given by the discrepancies between PMIP simulation and pollen data  
346 derived from a synthesis of the literature.

347 However, there are still some bias in the reconstruction. Estimated climates for the present  
348 day from IVM were compared with observed climates (Table 6), the slopes and intercepts show  
349 slightly bias for annual and January precipitation, while there is considerable bias between IVM  
350 reconstruction and observation for temperature and July precipitation. For the uncertainties on  
351 data reconstruction, IVM relies heavily on BIOME4, and since BIOME4 is a global vegetation  
352 model, it is possible that the spatial robustness of regional reconstruction could be less than that  
353 of global reconstruction due to the failure in simulating local features (Bartlein et al., 2011).  
354 Moreover, the output of the model is not directly compared to the pollen data, the conversion  
355 of BIOME4 biomes to pollen biomes by the transfer matrix may add the source of uncertainty  
356 in reconstruction. All these bias in reconstruction should be considered in the discrepancy  
357 between model-data for climate change during the MH over China.

#### 358 **4.2 Uncertainties for simulation**

359 Besides the qualitative consistency among models, caused by the protocol of PMIP3  
360 experiments (Table 2), a variability in the magnitude of anomalies between models is clearly  
361 illustrated by the boxplots (Fig.3 and Fig.4). These disparities in value or even pattern among  
362 models reflect the obvious differences in the response by the climate models to the MH forcing  
363 which raises on the question of the magnitude of feedbacks among models.

364 As positive feedbacks between climate and vegetation are important to explain regional  
365 climate changes, the failure to capture or the underestimation of the amplitude and pattern of  
366 the observed vegetation differences among models (see Section 3.2) could amplify and partly

367 account for the model-data disparities in climate change, mainly due to variations in the albedo.  
368 Because the HadGEM2-ES and HadGEM2-CC are the only two models in PMIP3 with  
369 dynamic vegetation simulation for the MH, we thus focused on them to examine the variations  
370 in vegetation fraction in the simulations. The main vegetation changes during the MH  
371 demonstrated by HadGEM2-ES are increased tree coverage (~15%) and a decreased bare soil  
372 fraction (~6%), while HadGEM2-CC depicts a ~3% decrease in tree fraction and a ~1%  
373 increase in bare soil (Fig. S9). We made a rough calculation of albedo variance caused solely by  
374 vegetation change for both two models and for our reconstruction, based on the area fraction  
375 and albedo value of each vegetation type (Betts, 2000; Bonfils et al., 2001; Oguntunde et al.,  
376 2006; Bonan, 2008).

377 The overall albedo change from the vegetation reconstruction during the MH shows a ~1.8%  
378 decrease when snow-free, with a much larger impact (~4.2% decrease) when snow-covered.  
379 The results from HadGEM2-ES are highly consistent with the albedo changes from the  
380 reconstruction, featuring a ~1.4% (~6.5%) decrease without (with) snow, while HadGEM2-CC  
381 produces an increased albedo value during the MH (~0.22% for snow-free, ~1.9% with  
382 snow-cover), depending on its vegetation simulation. Two ideas could be inferred from this  
383 calculation, 1) HadGEM2-ES is much better in simulating the MH vegetation changes than  
384 HadGEM2-CC. 2) the failure by models to capture these vegetation changes will result in a  
385 much larger impact on winter albedo (with snow) than summer albedo (without snow).

386 These surface albedo changes due to vegetation changes could have a cumulative effect on  
387 the regional climate by modifying the radiative fluxes. For instance, the spread of trees into the  
388 grassland biome in the northeast during the MH, revealed by the reconstruction in our study,  
389 should act as a positive feedback to climate warming by increasing the surface net shortwave  
390 radiation associated with reductions in albedo due to taller and darker canopies (Chapin et al.,  
391 2005). Previous studies show that cloud and surface albedo feedbacks on radiation are major



392 drivers of differences between model outputs for past climates. Moreover, the land surface  
393 feedback shows large disparities among models (Braconnot and Kageyama, 2015).

394 We used a simplified approach (Taylor et al., 2007) to quantify the feedbacks and to compare  
395 model behavior for the MH, thus justifying the focus on surface albedo and atmospheric  
396 scattering (mainly accounting for cloud change). Surface albedo and cloud change are  
397 calculated using the simulated incoming and outgoing radiative fluxes at the Earth's surface  
398 and at the top of atmosphere (TOA), based on data for the last 30 years averaged from all  
399 models. Using this framework, we quantified the effect of changes in albedo on the net  
400 shortwave flux at TOA (Braconnot and Kageyama, 2015), and further investigated the  
401 relationship between these changes and temperature change. Fig.8 shows that most models  
402 produced a negative cloud cover and surface albedo feedback on the annual mean shortwave  
403 radiative forcing. Concerning seasonal change, the shortwave cloud and surface feedback in  
404 most models tend to counteract the insolation forcing during the boreal summer, while they  
405 enhance the solar forcing during winter. A strong positive correlation between albedo feedback  
406 and temperature change is depicted, with a large spread in the models owing to the difference in  
407 albedo in the 13 models. In particular, CNRM-CM5 and HadGEM2-ES capture higher values  
408 of cloud and surface albedo feedback, which could be the reason for the reversal of the  
409 decreased annual temperature seen in other models (Fig. 3d).

410 However, the vegetation patterns produced by BIOME4 in Figure 5 are not used in PMIP3  
411 experiment setup, it's actually determined by the input variables from models. Previous study  
412 shows the GCMs from PMIP3 are reliable to simulate the geographical distribution of  
413 temperature and precipitation over China for present day without downscaling, but there is  
414 considerable bias between simulation and observation for precipitation (Jiang et al., 2016).  
415 Therefore, the disagreements of MH vegetation pattern possibly are inherited from the PI. To  
416 better quantify the vegetation-climate feedback, two experiments were conducted in CESM

417 version 1.0.5, including a mid-Holocene (MH) experiment (6 ka) with original vegetation  
418 setting (prescribed as PI vegetation for the MH) and a MH experiment with reconstructed  
419 vegetation (6 ka\_VEG). Figure 9 shows the climate anomalies (6 ka\_VEG minus 6 ka)  
420 between two simulations, for both annual and seasonal scale. For temperature, it's clear that  
421 the 6 ka\_VEG simulation reproduces a warmer annual mean climate (~0.3 K on average) as  
422 well as an obviously warmer winter (~0.6 K on average). For precipitation, the reconstructed  
423 vegetation leads to more annual and seasonal precipitation, which can also reconcile the  
424 discrepancy of increase amplitude for precipitation during the MH between model-data (data  
425 reproduced larger amplitude than model, revealed by our study). So the mismatch between  
426 model-data in MH vegetation could partly account for the discrepancy of climate due to the  
427 interaction between vegetation and climate through radiative and hydrological forcing with  
428 albedo. These results pinpoint the value of building a new generation of models able to capture  
429 not only the atmosphere and ocean response, but also the non-linear responses of vegetation and  
430 hydrology to the climate change.

## 431 **5. Conclusion**

432 In this study, we compare the annual and seasonal outputs from the PMIP3 models with an  
433 updated synthesis of climate reconstruction over China, including, for the first time, a seasonal  
434 cycle of temperature and precipitation. In response to the seasonal insolation change prescribed  
435 in PMIP3 for the MH, all models produce similar large-scale patterns for seasonal temperature  
436 and precipitation (higher than present July precipitation and MTWA, lower than present  
437 MTCO), with either an over- or underestimate of the climate changes when compared to the  
438 data. The main discrepancy emerging from the model-data comparison occurs in the annual and  
439 MTCO, where data show an increased value and most models simulate the opposite except  
440 CNRM-CM5 and HadGEM2-ES reproduced the higher-than-present annual temperature

441 during MH as data showed. By conducting simulations in BIOME4 and CESM, we show that  
442 the surface processes are the key factors drawing the uncertainties between models and data.  
443 These results pinpoint the crucial importance of including the non-linear responses of the  
444 surface water and energy balance to vegetation changes. Moreover, besides the vegetation  
445 influence, to which extent this model-data discrepancy is related to rough topography, soil type  
446 and other possible factors should be investigated in the future work.

447

448

#### 449 **Data availability**

450 The PMIP3 output is publicly available at website (<http://pmip3.lsce.ipsl.fr/>) by the climate  
451 modelling groups, the 65 pollen biomization results are provided by Members of China  
452 Quaternary Pollen Data Base, Table 1 shows the information (including references) of the 91  
453 collected pollen records and 3 original ones in our study, the biome scores of these 94 pollen  
454 records derived from IVM are listed in Table S4. All the reconstructed climate values at each  
455 pollen site from IVM are provided in Table S5.

#### 456 **Author contribution**

457 Yating Lin carried out the model-data analysis and prepared for the first manuscript, Gilles  
458 Ramstein contributed a lot to the paper's structure and content, Haibin Wu provided the  
459 reconstruction results from IVM and contributed the paper's structure and content. Raj  
460 Rani-Singh conducted the BIOME4 simulations. Ran Zhang carried out the simulation in  
461 CESM. Pascale Braconnot, Masa Kegeyama and Zhengtang Guo contributed great ideas on  
462 model-data comparison work. Qin Li and Yunli Luo provided pollen data. All co-authors  
463 helped to improve the paper.

464 **Competing interest**

465 The authors declare no competing interests.

466 **Acknowledgements**

467 We acknowledge the World Climate Research Program's Working Group on Coupled  
468 Modelling, which is responsible for PMIP/CMIP, and we thank the climate modelling groups  
469 for producing and making available their model output. We are grateful to Marie-France Loutre,  
470 Patrick Bartlein and three anonymous reviewers for constructive comments. This research was  
471 funded by the National Basic Research Program of China (Grant no. 2016YFA0600504), the  
472 National Natural Science Foundation of China (Grant nos. 41572165, 41690114, and  
473 41125011), the Sino-French Caiyuanpei Program, and the Bairen Programs of the Chinese  
474 Academy of Sciences.

475 **References**

476 An, C., Zhao, J., Tao, S., Lv, Y., Dong, W., Li, H., Jin, M., and Wang, Z.: Dust variation  
477 recorded by lacustrine sediments from arid Central Asia since ~ 15 cal ka BP and its  
478 implication for atmospheric circulation, *Quaternary Research*, 75, 566-573, 2011.

479 Bao, Q., Lin, P., Zhou, T., Liu, Y., Yu, Y., Wu, G., He, B., He, J., Li, L., Li, J., Li, Y., Liu, H.,  
480 Qiao, F., Song, Z., Wang, B., Wang, J., Wang, P., Wang, X., Wang, Z., Wu, B., Wu, T.,  
481 Xu, Y., Yu, H., Zhao, W., Zheng, W., and Zhou, L.: The flexible global  
482 ocean-atmosphere-land system model, spectral version 2: FGOALS-s2. *Advances in*  
483 *Atmospheric Sciences*, 30, 561-576, 2013.

484 Bartlein, P. J., Harrison, S. P., Brewer, S., Connor, S., Davis, B. A. S., Gajewski, K., Guiot, J.,  
485 Harrison-Prentice, T. I., Henderson, A., Peyron, O., Prentice, I. C., Scholze, M., Seppä, H.,  
486 Shuman, B., Sugita, S., Thompson, R. S., Viau, A. E., Williams, J., and Wu, H.B.:

487 Pollen-based continental climate reconstructions at 6 and 21ka: a global synthesis, *Climate*  
488 *Dynamics*, 37, 775-802, 2011.

489 Berger, A.: Long-Term Variations of Daily Insolation and Quaternary Climatic Changes,  
490 *Journal of the Atmospheric Sciences*, 35, 2362-2367, 1978.

491 Betts, R. A.: Offset of the potential carbon sink from boreal forestation by decreases in surface  
492 albedo, *Nature*, 408, 187-190, 2000.

493 Bigelow, N. H., Brubaker, L. B., Edwards, M. E., Harrison, S. P., Prentice, I. C., Anderson, P.  
494 M., Andreev, A. A., Bartlein, P. J., Christensen, T. R., Cramer, W., Kaplan, J. O., Lozhkin,  
495 A. V., Matveyeva, N. V., Murray, D. F., David McGuire, A., Razzhivin, V. Y., Ritchie, J. C.,  
496 Smith, B., Walker, A. D., Gajewski, K., Wolf, V., Holmqvist, B. H., Igarashi, Y.,  
497 Kremenetskii, K., Paus, A., Pisaric, M. F. J., and Volkova, V. S.: Climate change and Arctic  
498 ecosystems: 1. Vegetation changes north of 55°N between the last glacial maximum,  
499 mid-Holocene and present, *Journal of Geophysical Research*, 108, 1-25, 2003.

500 Bonan, G. B.: Forests and Climate Change: Forcings, Feedbacks, and the Climate Benefits of  
501 Forests, *Science*, 320, 1444-1449, 2008.

502 Bonfils, C., de Noblet-Ducoudré, N., Braconnot, P., and Joussaume, S.: Hot Desert Albedo and  
503 Climate Change: Mid-Holocene Monsoon in North Africa, *Journal of Climate*, 14,  
504 3724–3737, 2001.

505 Braconnot, P., and Kageyama, M.: Shortwave forcing and feedbacks in Last Glacial Maximum  
506 and Mid-Holocene PMIP3 simulations, *Philosophical Transactions of the Royal Society A:*  
507 *Mathematical, Physical and Engineering Sciences*, 373, 2054-2060, 2015.

508 Braconnot, P., Harrison, S. P., Kageyama, M., Bartlein, P. J., Masson-Delmotte, V., Abe-Ouchi,  
509 A., Otto-Bliesner, B., and Zhao, Y.: Evaluation of climate models using palaeoclimatic data:  
510 Nature Climate Change, 2, 417-421, 2012.

511 Braconnot, P., Otto-Bliesner, B., Harrison, S., Joussaume, S., Peterchmitt, J. Y., Abe-Ouchi, A.,  
512 Crucifix, M., Driesschaert, E., Fichefet, T., Hewitt, C. D., Kageyama, M., Kitoh, A., Laine,  
513 A., Loutre, M. F., Marti, O., Merkel, U., Ramstein, G., Valdes, P., Weber, S. L., Yu, Y., and  
514 Zhao, Y.: Results of PMIP2 coupled simulations of the Mid-Holocene and Last Glacial  
515 Maximum-Part 1: experiments and large-scale features, Climate of the Past, 3, 261-277,  
516 2007a.

517 Braconnot, P., Otto-Bliesner, B., Harrison, S., Joussaume, S., Peterschmitt, J. Y., Abe-Ouchi,  
518 A., Crucifix, M., Driesschaert, E., Fichefet, T., Hewitt, C. D., Kageyama, M., Kitoh, A.,  
519 Loutre, M. F., Marti, O., Merkel, U., Ramstein, G., Valdes, P., Weber, L., Yu, Y., and Zhao,  
520 Y.: Results of PMIP2 coupled simulations of the Mid-Holocene and Last Glacial  
521 Maximum-Part 2: feedbacks with emphasis on the location of the ITCZ and mid- and high  
522 latitudes heat budget, Climate of the Past, 3, 279-296, 2007b.

523 Cai, Y.: Study on environmental change in Zoige Plateau: Evidence from the vegetation  
524 record since 24000a B.P., Chinese Academy of Geological Sciences, Mater Dissertation,  
525 2008 (in Chinese with English abstract).

526 Caudill, M., Bulter, C.: Understanding Neural Networks, Basic Networks, 1, 309, 1992.

527 Chapin, F. S., Sturm, M., Serreze, M. C., McFadden, J. P., Key, J. R., Lloyd, A. H.,  
528 McGuire, A. D., Rupp, T. S., Lynch, A. H., Schimel, J. P., Beringer, J., Chapman, W. L.,  
529 Epstein, H. E., Euskirchen, E. S., Hinzman, L. D., Jia, G., Ping, C.L., Tape, K. D.,  
530 Thompson, C. D. C., Walker, D. A., and Welker, J. M.: Role of Land-Surface Changes in  
531 Arctic Summer Warming, Science, 310, 657-660, 2005.

532 Chen, F., Cheng, B., Zhao, Y., Zhu, Y., and Madsen, D. B.: Holocene environmental change  
533 inferred from a high-resolution pollen record, Lake Zhuyeze, arid China, *The Holocene*, 16,  
534 675-684, 2006.

535 Chen, F., Xu, Q., Chen, J., Birks, H. J. B., Liu, J., Zhang, S., Jin, L., An, C., Telford, R. J., Cao,  
536 X., Wang, Z., Zhang, X., Selvaraj, K., Lu, H., Li, Y., Zheng, Z., Wang, H., Zhou, A., Dong,  
537 G., Zhang, J., Huang, X., Bloemendal, J., and Rao, Z.: East Asian summer monsoon  
538 precipitation variability since the last deglaciation, *Scientific Reports*, 5, 1-11, 2015.

539 Cheng, B., Chen, F., and Zhang, J.: Palaeovegetational and Palaeoenvironmental Changes in  
540 Gonghe Basin since Last Deglaciation, *Acta Geographica Sinica*, 11, 1336-1344, 2010 (in  
541 Chinese with English abstract).

542 Cheng, H., Edwards, R. L., Sinha, A., Spötl, C., Yi, L., Chen, S., Kelly, M., Kathayat, G., Wang,  
543 X., Li, X., Kong, X., Wang, Y., Ning, Y., and Zhang, H.: The Asian monsoon over the past  
544 640,000 years and ice age terminations, *Nature*, 534, 640, 2016.

545 Cheng, Y.: Vegetation and climate change in the north-central part of the Loess Plateau since  
546 26,000 years, China University of Geosciences, Master Dissertation, 2011 (in Chinese  
547 with English abstract).

548 Collins, W. J., Bellouin, N., Doutriaux-Boucher, M., Gedney, N., Halloran, P., Hinton, T.,  
549 Hughes, J., Jones, C.D., Joshi, M., Liddicoat, S., Martin, G., O'Connor, F., Rae, J., Senior,  
550 C., Sitch, S., Totterdell, I., Wiltshire, A., and Woodward, S.: Development and evaluation  
551 of an Earth-system model—HadGEM2, *Geoscientific Model Development*, 4, 1051–1075,  
552 2011.

553 Cui, M., Luo, Y., and Sun, X.: Paleovegetational and paleoclimatic changed in Ha'ni Lake,  
554 Jilin since 5ka BP, *Marine Geology & Quaternary Geology*, 26, 117-122, 2006 (in  
555 Chinese with English abstract).

556 Dallmeyer, A., Claussen, M., Ni, J., Cao, X., Wang, Y., Fischer, N., Pfeiffer, M., Jin, L.,  
557 Khon, V., Wagner, S., Haberkorn, K., and Herzschuh, U.: Biome changes in Asia since  
558 the mid-Holocene and analysis of difference transient Earth system model simulations,  
559 *Climate of the Past*, 13, 107-134, 2017.

560 Davis, B. A. S., Brewer, S., Stevenson, A. C., and Guiot, J.: The temperature of Europe during  
561 the Holocene reconstructed from pollen data, *Quaternary Science Reviews*, 22, 1701-1716,  
562 2003.

563 Diffenbaugh, N.S., Sloan, L.C., Snyder, M.A., Bell, J.L., Kaplan, J., Shafer, S.L., and Bartlein,  
564 P.J.: Vegetation sensitivity to global anthropogenic carbon dioxide emissions in a  
565 topographically complex region, *Global Biogeochemical Cycles*, 17, 1067,  
566 doi:10.1029/2002GB001974, 2003.

567 Dufresne, J.L., Foujols, M.A., Denvil, S., Caubel, A., Marti, O., Aumont, O., Balkanski, Y.,  
568 Bekki, S., Bellenger, H., Benshila, R., Bony, S., Bopp, L., Braconnot, P., Brockmann, P.,  
569 Cadule, P., Cheruy, F., Codron, F., Cozic, A., Cugnet, D., Noblet, N., Duvel, J.P., Ethe, C.,  
570 Fairhead, L., Fichefet, T., Flavoni, S., Friedlingstein, P., Grandpeix, J.Y., Guez, L.,  
571 Guilyardi, E., Hauglustaine, D., Hourdin, F., Idelkadi, A., Ghattas, J., Joussaume, S.,  
572 Kageyama, M., Krinner, G., Labetoulle, S., Lahellec, A., Lefevre, M.-F., Lefevre, F.,  
573 Levy, C., Li, Z.X., Lloyd, J., Lott, F., Madec, G., Mancip, M., Marchand, M., Masson, S.,  
574 Meurdesoif, Y., Mignot, J., Musat, I., Parouty, S., Polcher, J., Rio, C., Schulz, M.,  
575 Swingedouw, D., Szopa, S., Talandier, C., Terray, P., Viovy, N., and Vuichard, N.:  
576 Climate change projections using the IPSL-CM5 Earth system model: from CMIP3 to  
577 CMIP5, *Climate Dynamics*, 40, 2123-2165, 2013.

578 EPICA Community Members: Eight glacial cycles from an Antarctic ice core, *Nature*, 429,  
579 623-628, 2004.



580 Food and Agricultural organization: Soil Map of the World 1:5000,000. 1995.

581 Farrera, I., Harrison, S. P., Prentice, I. C., Ramstein, G., Guiot, J., Bartlein, P. J., Bonnefille, R.,  
582 Bush, M., Cramer, W., von Grafenstein, U., Holmgren, K., Hooghiemstra, H., Hope, G.,  
583 Jolly, D., Lauritzen, S. E., Ono, Y., Pinot, S., Stute, M., and Yu, G.: Tropical climates at the  
584 Last Glacial Maximum: a new synthesis of terrestrial palaeoclimate data. I. Vegetation,  
585 lake-levels and geochemistry, *Climate Dynamics*, 15, 823-856, 1999.

586 Fischer, N., and Jungclaus, J. H.: Evolution of the seasonal temperature cycle in a transient  
587 Holocene simulation: orbital forcing and sea-ice, *Climate of the Past*, 7, 1139-1148, 2011.

588 Ganopolski, A., Kubatzki, C., Claussen, M., Brovkin, V., and Petoukhov, V.: The Influence of  
589 Vegetation-Atmosphere-Ocean Interaction on Climate during the Mid-Holocene, *Science*,  
590 280, 1916-1919, 1998.

591 Gent, P.R., Danabasoglu, G., Donner, L.J., Holland, M.M., Hunke, E.C., Jayne, S.R.,  
592 Lawrence, D.M., Neale, R.B., Rasch, P.J., Vertenstein, M., Worley, P.H., Yang, Z., and  
593 Zhang, M.: The community climate system model version 4, *Journal of Climate*, 24,  
594 4973-4991, 2011.

595 Giorgetta, M.A., Jungclaus, J., Reick, C.H., Legutke, S., Bader, J., Bottinger, M., Brovkin, V.,  
596 Crueger, T., Esch, M., Fieg, K., Glushak, K., Gayler, V., Haak, H., Hollweg, H.D., Ilyina,  
597 T., Kinne, S., Kornblueh, L., Matei, D., Mauritsen, T., Mikolajewicz, U., Mueller, W.,  
598 Notz, D., Pithan, F., Raddatz, T.J., Rast, S., Redler, R., Roeckner, E., Schmidt, H., Schnur,  
599 R., Segschneider, J., Six, K.D., Stockhause, M., Timmreck, C., Wegner, J., Widmann, H.,  
600 Wieners, K.H., Claussen, M., Marotzke, J., and Stevens, B.: Climate and carbon cycle  
601 changes from 1850 to 2100 in MPI-ESM simulations for the Coupled Model  
602 Intercomparison Project phase 5, *Journal of Advances in Modeling Earth System*, 5,  
603 572-597, 2013.

604 Gong, X.: High-resolution paleovegetation reconstruction from pollen in Jiachuanyuan, Baoji,  
605 Capital Normal University, Master Dissertation, 2006 (in Chinese with English abstract).

606 Guiot, J., and Goeury, C.: PPPBASE, a software for statistical analysis of paleoecological and  
607 paleoclimatological data, *Dendrochronologia*, 14, 295-300, 1996.

608 Guiot, J., Harrison, S., and Prentice, I. C.: Reconstruction of Holocene precipitation patterns in  
609 Europe using pollen and lake level data, *Quaternary Research*, 40, 139-149, 1993.

610 Guiot, J., Torre, F., Jolly, D., Peyron, O., Boreux, J. J., and Cheddadi, R.: Inverse vegetation  
611 modeling by Monte Carlo sampling to reconstruct palaeoclimates under changed  
612 precipitation seasonality and CO<sub>2</sub> conditions: application to glacial climate in  
613 Mediterranean region, *Ecological Modelling*, 127, 119-140, 2000.

614 Guo, L., Feng, Z., Lee, X., Liu, L., and Wang, L.: Holocene climatic and environmental  
615 changes recorded in Baahar Nuur Lake in the Ordos Plateau, Southern Mongolia of china,  
616 *Chinese Science Bulletin*, 52, 959-966, 2007.

617 Hargreaves, J. C., Annan, J. D., Ohgaito, R., Paul, A., and Abe-Ouchi, A.: Skill and reliability  
618 of climate model ensembles at the Last Glacial Maximum and mid-Holocene, *Climate of  
619 the Past*, 9, 811-823, 2013.

620 Harrison, S. P., Bartlein, P. J., Brewer, S., Prentice, I. C., Boyd, M., Hessler, I., Holmgren, K.,  
621 Izumi, K., and Willis, K.: Climate model benchmarking with glacial and mid-Holocene  
622 climates, *Climate Dynamics*, 43, 671-688, 2014.

623 Harrison, S. P., Bartlein, P. J., K., Izumi, Li, G., Annan, J., Hargreaves, J., Braconnot, P., and  
624 Kageyama, M.: Evaluation of CMIP5 paleo-simulations to improve climate projections,  
625 *Nature Climate Change*, 5, 735-743, 2015.

- 626 Harrison, S., P., Braconnot, P., Hewitt, C., and Stouffer, R., J.: Fourth International Workshop  
627 of the Palaeoclimate Modelling Intercomparison Project (PMIP): Lauching PMIP2 Phase II,  
628 EOS, 83, 447-457, 2002.
- 629 Herzschuh, U., Kramer, A., Mischke, S., and Zhang, C.: Quantitative climate and vegetation  
630 trends since the late glacial on the northeastern Tibetan Plateau deduced from Koucha  
631 Lake pollen spectra, Quaternary Research, 71, 162-171, 2009.
- 632 Herzschuh, U., Kürschner, H., and Mischke, S.: Temperature variability and vertical  
633 vegetation belt shifts during the last ~50,000 yr in the Qilian mountains (NE margin of  
634 the Tibetan Plateau, China), Quaternary Research, 66, 133-146, 2006.
- 635 Huang, C., Elis, V. C., and Li, S.: Holocene environmental changes of Western and Northern  
636 Qinghai-Xizang Plateau Based on pollen analysis, Acta Micropalaeontologica Sinica, 4,  
637 423-432, 1996 (in Chinese with English abstract).
- 638 Jeffrey, S.J., Rotstayn, L.D., Collier, M., Dravitzki, S.M., Hamalainen, C., Moeseneder, C.,  
639 Wong, K.K., and Syktus, J.I.: Australia' s CMIP5 submission using the CSIRO-Mk3.6  
640 model, Australian Meteorological and Oceanographic Journal, 63, 1-13, 2013.
- 641 Jia, L., and Zhang, Y.: Studies on Palynological assemblages and paleoenvironment of late  
642 Quaternary on the east margin of the Chanjiang (Yangtze) river delta, Acta  
643 Micropalaeontologica Sinica, 23, 70-76, 2006 (in Chinese with English abstract).
- 644 Jiang, D., Lang, X., Tian, Z., and Wang, T.: Considerable Model–Data Mismatch in  
645 Temperature over China during the Mid-Holocene: Results of PMIP Simulations, Journal  
646 of Climate, 25, 4135-4153, 2012.
- 647 Jiang, D., Tian, Z., and Lang, X.: Mid-Holocene net precipitation changes over China:  
648 model-data comparison, Quaternary Science Reviews, 82, 104-120, 2013.

649 Jiang, D., Tian, Z., and Lang, X.: Reliability of climate models for China through the IPCC  
650 Third to Fifth Assessment Reports, *International Journal of Climatology*, 36, 1114-1133,  
651 2016.

652 Jiang, Q., and Piperno., R. D.: Environmental and archaeological implications of a late  
653 Quaternary palynological sequence, Poyang lake, Southern China, *Quaternary Research*,  
654 52, 250-258, 1999.

655 Jiang, W., Guiot, J., Chu, G., Wu, H., Yuan, B., Hatté, C., and Guo, Z.: An improved  
656 methodology of the modern analogues technique for palaeoclimate reconstruction in arid  
657 and semi-arid regions, *Boreas*, 39, 145-153, 2010.

658 Jiang, W., Guo, Z., Sun, X., Wu, H., Chu, G., Yuan, B., Hatte, C., and Guiot, J.:  
659 Reconstruction of climate and vegetation changes of Lake Bayanchagan (Inner Mongolia):  
660 Holocene variability of the East Asian monsoon. *Quaternary Research*, 65, 411-420, 2006.

661 Jiang, W., Leroy, S. G., Ogle, N., Chu, G., Wang, L., and Liu, J.: Natural and authropogenic  
662 forest fires recorded in the Holocene pollen record from a Jinchuan peat bog, northeastern  
663 China, *Palaeogeography, Palaeoclimatology, Palaeoecology*, 261, 47-57, 2008.

664 Joussaume, S., and Taylor, K. E.: Status of the Paleoclimate Modeling Intercomparison Project,  
665 *Proceedings of the First International AMIP Scientific Conference*, 425-430, 1995.

666 Joussaume, S., Taylor, K. E., Braconnot, P., Mitchell, J. F. B., Kutzbach, J. E., Harrison, S. P.,  
667 Prentice, I. C., Broccoli, A. J., Abe-Ouchi, A., Bartlein, P. J., Bonfils, C., Dong, B., Guiot,  
668 J., Herterich, K., Hewitt, C. D., Jolly, D., Kim, J. W., Kislov, A., Kitoh, A., Loutre, M. F.,  
669 Masson, V., McAvaney, B., McFarlane, N., de Noblet, N., Peltier, W. R., Peterschmitt, J. Y.,  
670 Pollard, D., Rind, D., Royer, J. F., Schlesinger, M. E., Syktus, J., Thompson, S., Valdes, P.,  
671 Vettoretti, G., Webb, R. S., Wyputta, U.: Monsoon changes for 6000 years ago: Results of

672 18 simulations from the Paleoclimate Modeling Intercomparison Project (PMIP),  
673 Geophysical Research Letters, 26, 856-862, 1999.

674 Kaplan, J. O., Bigelow, N. H., Bartlein, P. J., Christensen, T. R., Cramer, W., Harrison, S. P.,  
675 Matveyeva, N. V., McGuire, A. D., Murray, D. F., Prentice, I. C., Razzhivin, V. Y., Smith,  
676 B., Anderson, P. M., Andreev, A. A., Brubaker, L. B., Edwards, M. E., and Lozhkin, A. V.:  
677 Climate change and Arctic ecosystems: 2. Modeling, palaeodata-model comparisons, and  
678 future projections, Journal of Geophysical Research: Atmospheres, 108, 8171,  
679 doi:10.1029/2002JD002559, 2003.

680 Kohfeld, K. E. and Harrison, S.: How well we can simulate past climates? Evaluating the  
681 models using global palaeoenvironmental datasets, Quaternary Science Reviews, 19,  
682 321-346, 2000.

683 Kong, Z., Xu, Q., Yang, X., Sun, L., Liang, W.: Analysis of sporopollen assemblages of  
684 Holocene alluvial deposits in the Yinmahe River Basin, Hebei Province, and preliminary  
685 study on temporal and spatial changes of vegetation, Acta Phytocologica Sinica, 24, 724,  
686 2000 (in Chinese with English abstract).

687 Lee, Y., and Liew, M.: Pollen stratigraphy, vegetation and environment of the last glacial and  
688 Holocene-A record from Toushe Basin, central Taiwan,  
689 Palaeogeography, Palaeoclimatology, Palaeoecology, 287, 58-66, 2010.

690 Li, B., and Sun, J.: Vegetation and climate environment during Holocene in Xi'an region of  
691 Loess Plateau, China, Marine Geology and Quaternary Geology, 3, 125-132, 2005 (in  
692 Chinese with English abstract).

693 Li, C., Wu, Y., and Hou, X.: Holocene vegetation and climate in Northeast China revealed  
694 from Jingbo Lake sediment, Quaternary International, 229, 67-73, 2011.

695 Li, L., Lin, P., Yu, Y., Wang, B., Zhou, T., Liu, L., Liu, J., Bao, Q., Xu, S., Huang, W., Xia,  
696 K., Pu, Y., Dong, L., Shen, S., Liu, Y., Hu, N., Liu, M., Sun, W., Shi, X., Zheng, W., Wu,  
697 B., Song, M., Liu, H., Zhang, X., Wu, G., Xue, W., Huang, X., Yang, G., Song, Z., and  
698 Qiao, F.: The flexible global ocean-atmosphere-land system model, Grid-point Version 2:  
699 FGOALS-g2, *Advances in Atmospheric Sciences*, 30, 543-560, 2013.

700 Li, Q., Wu, H., Guo, Z., Yu, Y., Ge, J., Wu, J., Zhao, D., and Sun, A.: Distribution and  
701 vegetation reconstruction of the deserts of northern China during the mid-Holocene,  
702 *Geophysical Research Letter*, 41, 2184-5191, 2014.

703 Li, X., and Liu, J.: Holocene vegetational and environmental changes at Mt. Luoji, Sichuan,  
704 *Acta Geographica Sinica*, 1, 44-51, 1988 (in Chinese with English abstract).

705 Li, X., Zhao, K., Dodson, J., and Zhou, X.: Moisture dynamics in central Asia for the last  
706 15 kyr: new evidence from Yili Valley, Xinjiang, NW China, *Quaternary Science*  
707 *Reviews*, 30, 23-34, 2011.

708 Li, X., Zhou, J., and Dodson, J.: The vegetation characteristics of the ‘yuan’ area at Yaoxian  
709 on the loess plateau in china over the last 12 000 years. *Review of Palaeobotany &*  
710 *Palynology*, 124, 1-7, 2003.

711 Li, X., Zhou, W., An, Z., and Dodson, J.: The vegetation and monsoon variations at the  
712 desert-loess transition belt at Midiwan in northern China for the last 13 ka, *Holocene*, 13,  
713 779-784, 2003.

714 Li, Z., Hai, Y., Zhou, Y., Luo, R., Zhang, Q.: Pollen Component of Lacustrain Deposit and its  
715 Palaeo-environment Significance in the Downstream Region of Urumqi Riever since  
716 30Ka BP, *Arid Land Geography*, 24, 201-205, 2001 (in Chinese with English abstract).

- 717 Liu, H., Cui, H., Tian, Y., and Xu, L.: Temporal-spatial variances of Holocene precipitation at  
718 the Marginal area of the East Monsoon influences from pollen evidence, *Acta Botanica*  
719 *Sinica*, 44, 864-871, 2002 (in Chinese with English abstract).
- 720 Liu, H., Tang, X., Sun, D., and Wang, K.: Palynofloras of the Dajiuhu Basin in Shennongjia  
721 mountains during the last 12.5 ka, *Acta Micropalaeontologica Sinica*, 1, 101-109, 2001 (in  
722 Chinese with English abstract).
- 723 Liu, J., Zhao, S., Cheng, J., Bao, J., and Yin, G.: A study of vegetation and climate evolution  
724 since the Holocene near the banks of the Qiangtang River in Hangzhou Bay, *Earth*  
725 *Science Frontiers*, 5, 235-245, 2007 (in Chinese with English abstract).
- 726 Liu, M., Huang, Y., and Kuo, M.: Pollen stratigraphy, vegetation and environment of the last  
727 glacial and Holocene-A record from Toushe Basin, central Taiwan, *Quaternary*  
728 *International*, 14, 16-33, 2006.
- 729 Liu, Y., Liu, J., and Han, J.: Pollen record and climate changing since 12.0ka B. P. in  
730 Erlongwan Maar Lake, Jilin province, *Journal of Jilin University (Earth Science Edition)*,  
731 39, 93-98, 2009 (in Chinese with English abstract).
- 732 Liu, Y., Zhang, S., Liu, J., You, H., and Han, J.: Vegetation and environment history of  
733 erlongwan Maar lake during the late Pleistocene on pollen record, *Acta*  
734 *Micropalaeontologica Sinica*, 25, 274-280, 2008 (in Chinese with English abstract).
- 735 Liu, Z., Harrison, S. P., Kutzbach, J. E., and Otto-Bliesner, B.: Global monsoons in the  
736 mid-Holocene and oceanic feedback, *Climate Dynamics*, 22, 157-182, 2004.
- 737 Liu, Z., Wang, Y., Gallimore, R., Gasse, F., Johnson, T., deMenocal, P., Adkins, J., Notaro, M.,  
738 Prentice, I.C., Kutzbach, J., Jacob, R., Behling, P., Wang, L., and Ong, E.: Simulating the

739 transient evolution and abrupt change of Northern Africa atmosphere–ocean–terrestrial  
740 ecosystem in the Holocene, *Quaternary Science Reviews*, 26, 1818-1837, 2007.

741 Liu, Z., Zhu, J., Rosenthal, Y., Zhang, X., Otto-Bliesner, B. L., Timmermann, A., Smith, R. S.,  
742 Lohmann, G., Zheng, W., and Elison Timm, O.: The Holocene temperature conundrum,  
743 *Proceedings of the National Academy of Sciences*, 111, E3501-E3505, 2014.

744 Lu, H., Wu, N., Liu, K.-b., Zhu, L., Yang, X., Yao, T., Wang, L., Li, Q., Liu, X., Shen, C., Li, X.,  
745 Tong, G., and Jiang, H.: Modern pollen distributions in Qinghai-Tibetan Plateau and the  
746 development of transfer functions for reconstructing Holocene environmental changes,  
747 *Quaternary Science Reviews*, 30, 947-966, 2012.

748 Luo, H.: Characteristics of the Holocene sporopollen flora and climate change in the Coqên  
749 area, Tibet, Chengdu University of Technology, Master Dissertation, 2008 (in Chinese  
750 with English abstract).

751 Mann, M. E., Zhang, Z., Hughes, M. K., Bradley, R. S., Miller, S. K., Rutherford, S., and Ni, F.:  
752 Proxy-based reconstructions of hemispheric and global surface temperature variations over  
753 the past two millennia, *Proceedings of the National Academy of Sciences*, 105,  
754 13252-13256, 2008.

755 Marchant, R., Cleef, A., Harrison, S. P., Hooghiemstra, H., Markgraf, V., Van Boxel, J., Ager,  
756 T., Almeida, L., Anderson, R., Baied, C., Behling, H., Berrio, J. C., Burbridge, R., Bjorck,  
757 S., Byrne, R., Bush, M., Duivenvoorden, J., Flenley, J., De Oliveira, P., Van Gee, B., Graf,  
758 K., Gosling, W. D., Harbele, S., Van Der Hammen, T., Hansen, B., Horn, S., Kuhry, P.,  
759 Ledru, M. P., Mayle, F., Leyden, B., Lozano-Garcia, S., Melief, A. M., Moreno, P., Moar,  
760 N. T., Prieto, A., Van Reenen, G., Salgado-Labouriau, M., Schabitz, F., Schreve-Brinkman,  
761 E. J., and Wille, M.: Pollen-based biome reconstructions for Latin America at 0, 6000 and  
762 18 000 radiocarbon years ago, *Climate of the Past*, 5, 725-767, 2009.



763 Marcott, S., Shakun, J., U Clark, P., and Mix, A.: A Reconstruction of Regional and Global  
764 Temperature for the Past 11,300 Years, *Science*, 1198-1201, 2013.

765 Mauri, A., Davis, B. A. S., Collins, P. M., and Kaplan, J. O.: The climate of Europe during the  
766 Holocene: a gridded pollen-based reconstruction and its multi-proxy evaluation,  
767 *Quaternary Science Reviews*, 112, 109-127, 2015.

768 Ma, Y., Zhang, H., Pachur, H., Wunnemann, B., Li, J., and Feng, Z.: Late Glacial and  
769 Holocene vegetation history and paleoclimate of the Tengger Desert, northwestern China,  
770 *Chinese Science Bulletin*, 48, 1457-1463, 2003.

771 Members of the China Quaternary Pollen Data Base.: Pollen-based Biome reconstruction at  
772 Middle Holocene (6 ka BP) and Last Glacial Maximum (18 ka BP) in China, *Acta Botanica*  
773 *Sinica*, 42, 1201-1209, 2000.

774 Members, M. P.: Constraints on the magnitude and patterns of ocean cooling at the Last Glacial  
775 Maximum, *Nature Geoscience*, 2, 127-130, 2009.

776 Meng, X., Zhu, D., Shao, Z., Han, J., Yu, J., Meng, Q., Lv, R., and Luo, P.: Paleoclimatic and  
777 Palaeoenvironmental Evolution Since Holocene in the Ningwu Area, Shanxi Province, *Acta*  
778 *Geologica Sinica*, 3, 316-323, 2007 (in Chinese with English abstract).

779 Ni, J., Sykes, M. T., Prentice, I. C., and Cramer, W.: Modelling the vegetation of China using  
780 the process-based equilibrium terrestrial biosphere model BIOME3, *Global Ecology and*  
781 *Biogeography*, 9, 463-479, 2000.

782 Ni, J., Yu, G., Harrison, S.P., Prentice, I. C.: Palaeovegetation in China during the late  
783 Quaternary: Biome reconstructions based on a global scheme of plant functional types,  
784 *Palaeogeography, Palaeoclimatology, Palaeoecology*, 289, 44-61, 2010.

785 Oguntunde, P. G., Ajayi, A. E., and Giesen, N.: Tillage and surface moisture effects on  
786 bare-soil albedo of a tropical loamy sand, *Soil and Tillage Research*, 85, 107-114, 2006.

787 O'ishi, R., Abe - Ouchi, I. C. Prentice, and S. Sitch.: Vegetation dynamics and plant CO<sub>2</sub>  
788 responses as positive feedbacks in a greenhouse world, *Geophysical Research Letters*, 36,  
789 L11706, doi: 10.1029/2009GL038217, 2009.

790 Otto, J., T. Raddatz, M. Claussen, V. Brovkin, and V. Gayler.: Separation of  
791 atmosphere-ocean-vegetation feedbacks and synergies for mid-Holocene climate,  
792 *Geophysical Research Letters*, 36, L09701, doi: 10.1029/2009GL037482, 2009.

793 Peyron, O., Guiot, J., Cheddadi, R., Tarasov, P., Reille, M., De Beaulieu, J.L., Bottema, S., and  
794 Andrieu, Valerie. : Climatic reconstruction in Europe for 18,000 YR B.P. from pollen data,  
795 *Quaternary Research*, 49, 183-196, 1998.

796 Peyron, O., Jolly, D., Bonnefille, R., Vincens, A., and Guiot, J.: Climate of East Africa 6000  
797 <sup>14</sup>C yr B.P. as Inferred from Pollen Data, *Quaternary Research*, 54, 90-101, 2000.

798 Pickett Elizabeth, J., Harrison Sandy, P., Hope, G., Harle, K., Dodson John, R., Peter Kershaw,  
799 A., Colin Prentice, I., Backhouse, J., Colhoun Eric, A., D'Costa, D., Flenley, J., Grindrod, J.,  
800 Haberle, S., Hassell, C., Kenyon, C., Macphail, M., Martin, H., Martin Anthony, H.,  
801 McKenzie, M., Newsome Jane, C., Penny, D., Powell, J., Ian Raine, J., Southern, W.,  
802 Stevenson, J., Sutra, J. P., Thomas, I., Kaars, S., and Ward, J.: Pollen-based reconstructions  
803 of biome distributions for Australia, Southeast Asia and the Pacific (SEAPAC region) at 0,  
804 6000 and 18,000 <sup>14</sup>C yr BP, *Journal of Biogeography*, 31, 1381-1444, 2004.

805 Prentice, I. C., Guiot, J., Huntley, B., Jolly, D., and Cheddadi, R.: Reconstructing biomes from  
806 palaeoecological data: A general method and its application to European pollen data at 0  
807 and 6 ka, *Climate Dynamics*, 12, 185-194, 1996.

808 Prentice, I. C., and Jolly, D.: Mid-Holocene and glacial-maximum vegetation geography of the  
809 northern continents and Africa, *Journal of Biogeography*, 27, 507-519, 2000.

810 Schmidt, G.A., Annan, J.D., Bartlein, P.J., Cook, B.I., Guilyardi, E., Hargreaves, J.C.,  
811 Harrison, S.P., Kageyama, M., Legrande, A.N., Konecky, B.L., Lovejoy, S., Mann, M.E.,  
812 Masson-Delmotte, V., Risi, C., Thompson, D., Timmermann, A., and Yiou, P.: Using  
813 palaeo-climate comparisons to constrain future projections in CMIP5, *Climate of the Past*,  
814 10, 221-250, 2014a.

815 Schmidt, G.A., Kelley, M., Nazarenko, L., Ruedy, R., Russell, G.L., Aleinov, I., Bauer, M.,  
816 Bauer, S.E., Bhat, M.K., Bleck, R., Canuto, V., Chen, Y., Cheng, Y., Clune, T.L., Del  
817 Genio, A., de Fainchtein, R., Faluvegi, G., Hansen, J.E., Healy, R.J., Kiang, N.Y., Koch,  
818 D., Lacis, A.A., Legrande, A.N., Lerner, J., Lo, K.K., Matthews, E.E., Menon, S., Miller,  
819 R.L., Oinas, V., Oloso, A.O., Perlwitz, J.P., Puma, M.J., Putman, W.M., Rind, D.,  
820 Romanou, A., Sato, M., Shindell, D.T., Sun, S., Syed Rahman, A., Tausnev, N., Tsigaridis,  
821 K., Under, N., Voulgarakis, A., Yao, M., and Zhang, J.: Configuration and assessment of  
822 the GISS ModelE2 contributions to the CMIP5 archive, *Journal of Advances in Modeling  
823 Earth Systems*, 6, 141-184, 2014b.

824 Shakun, J. D., Clark, P. U., He, F., Marcott, S. A., Mix, A. C., Liu, Z., Otto-Bliesner, B.,  
825 Schmittner, A., and Bard, E.: Global warming preceded by increasing carbon dioxide  
826 concentrations during the last deglaciation, *Nature*, 484, 49-55, 2012.

827 Shen, C., Liu, K., Tang, L., Overpeck, J. T.: Quantitative relationships between modern  
828 pollen rain and climate in the Tibetan Plateau, *Review of Palaeobotany and Palynology*,  
829 140, 61-77, 2006.

830 Shen, J., Jones, R. T., Yang, X., Dearing, J. A., and Wang, S.: The Holocene vegetation  
831 history of lake Erhai, Yunnan province southwestern china: the role of climate and human  
832 forcings, *The Holocene*, 16, 265-276, 2006.

833 Shen, J., Liu, X., Matsumoto, R., Wang, S., Yang, X., Tang, L., and Shen, C.: Multi-index  
834 high-resolution paleoclimatic evolution of sediments in Qinghai Lake since the late glacial  
835 period, *Science in China Series D: Earth Sciences*, 6, 582-589, 2004 (in Chinese with  
836 English abstract).

837 Shu, J., Wang, W., and Chen, Y.: Holocene vegetation and environment changes in the NW  
838 Taihu Plain, Jiangsu Province, East China, *Acta Micropalaeontologica Sinica*, 2, 210-221,  
839 2007 (in Chinese with English abstract).

840 Shu, Q., Xiao, J., Zhang, M., Zhao, Z., Chen, Y., and Li, J.: Climate Change in Northern  
841 Jiangsu Basin since the Last Interglacial: *Geological Science and Technology Information*,  
842 5, 59-64, 2008 (in Chinese with English abstract).

843 Song, M., Zhou, C., and Ouyang, H.: Simulated distribution of vegetation types in response to  
844 climate change on the Tibetan Plateau, *Journal of Vegetation Science*, 16, 341-350, 2005.

845 Sun, A., and Feng, Z.: Holocene climate reconstructions from the fossil pollen record at Qigai  
846 Nuur in the southern Mongolian Plateau, *The Holocene*, 23, 1391-1402, 2013.

847 Sun, L., Xu, Q., Yang, X., Liang, W., Sun, Z., and Chen, S.: Vegetation and environmental  
848 changes in the Xuanhua Basin of Hebei Province since Postglacial, *Journal of*  
849 *Geomechanics*, 4, 303-308, 2001 (in Chinese with English abstract).

850 Sun, Q., Zhou, J., Shen, J., Cheng, P., Wu, F., and Xie, X.: Mid-Holocene environmental  
851 characteristics recorded in the sediments of the Bohai Sea in the northern environmental

852 sensitive zone, *Science in China Series D: Earth Sciences*, 9, 838-849, 2006 (in Chinese  
853 with English abstract).

854 Sun, X., and Xia, Z.: Paleoenvironment Changes Since Mid-Holocene Revealed by a  
855 Palynological Sequence from Sihenan Profile in Luoyang, Henan Province, *Acta*  
856 *Scientiarum Naturalium Universitatis Pekinensis*, 2, 289-294, 2005 (in Chinese with  
857 English abstract).

858 Sun, X., Wang, F., and Sun, C.: Pollen-climate response surfaces of selected taxa from  
859 Northern China, *Science in China Series D: Earth Sciences*, 39, 486, 1996.

860 Swann, A. L., Fung, I. Y., Levis, S., Bonan, G. B., and Doney, S. C.: Changes in Arctic  
861 vegetation amplify high-latitude warming through the greenhouse effect, *Proceedings of*  
862 *the National Academy of Sciences*, 107, 1295-1300, 2010.

863 Sykes, M.T., Prentice, I.C., and Laarif, F.: Quantifying the impact of global climate change on  
864 potential natural vegetation, *Climatic Change*, 41, 37–52, 1999.

865 Tang, L., and An, C.: Holocene vegetation change and pollen record of drought events in the  
866 Loess Plateau, *Progress in Natural Science*, 10, 1371-1382, 2007 (in Chinese with English  
867 abstract).

868 Tang, L., and Shen, C.: Holocene pollen records of the Qinghai-Xizang Plateau, *Acta*  
869 *Micropalaeontologica Sinica*, 4, 407-422, 1996 (in Chinese with English abstract).

870 Tang, L., Shen, C., Kong, Z., Wang, F., and Liao, K.: Pollen evidence of climate during the  
871 last glacial maximum in Eastern Tibetan Plateau, *Journal of Glaciology*, 2, 37-44, 1998  
872 (in Chinese with English abstract).

873 Tang, L., Shen, C., Li, C., Peng, J., and Liu, H.: Pollen-inferred vegetation and environmental  
874 changes in the central Tibetan Plateau since 8200 yr B.P., *Science in China Series D:  
875 Earth Sciences*, 5, 615-625, 2009 (in Chinese with English abstract).

876 Tao, S., An, C., Chen, F., Tang, L., Wang, Z., Lv, Y., Li, Z., Zheng, T., and Zhao, J.:  
877 Vegetation and environment since the 16.7cal ka B.P. in Balikun Lake, Xinjiang, China,  
878 *Chinese Science Bulletin*, 11, 1026-1035, 2010 (in Chinese with English abstract).

879 Taylor, K.E., Crucifix, M., Braconnot, P., Hewitt, C. D., Doutriaux. C., Broccoli, A. J., Mitchell,  
880 J. F. B., Webb, M. J.: Estimating shortwave radiative forcing and response in climate  
881 models, *Journal of Climate*, 20, 2530-2543, 2007.

882 Taylor, K.E., Stouffer, R.J., Meehl, G.A.: An overview of CMIP5 and the experiment design,  
883 *Bulletin of the American Meteorological Society*, 93, 485-498, 2012.

884 Voldoire, A., Sanchez-Gomez, E., Salas y Melia, D., Decharme, B., Cassou, C., Senesi, S.,  
885 Valcke, S., Beau, I., Alias, A., Chevallier, M., Deque, M., Deshayes, J., Douville, H.,  
886 Fernandez, E., Madec, G., Maisonnave, E., Moine, M., Planton, S., Saint-Martin, D.,  
887 Szopa, S., Tyteca, S., Alkama, R., Belamari, S., Braun, A., Coquart, L., and Chauvin, F.:  
888 The CNRM-CM5.1 global climate model: description and basic evaluation, *Climate  
889 Dynamics*, 40, 2091-2121, 2012.

890 Wang, H., Liu, H., Zhu, J., and Yin, Y.: Holocene environmental changes as recorded by  
891 mineral magnetism of sediments from Anguli-nuur Lake, southeastern Inner Mongolia  
892 Plateau, China, *Palaeogeography, Palaeoclimatology, Palaeoecology*, 285, 30-49, 2010.

893 Wang, S., Lv, H., and Liu, J.: Environmental characteristics of the early Holocene suitable  
894 period revealed by the high-resolution sporopollen record of Huguangyan Lake, *Chinese  
895 Science Bulletin*, 11, 1285-1291, 2007 (in Chinese with English abstract).

896 Wang, X., Wang, J., Cao, L., Yang, J., Yang, X., Peng, Z., and Jin, G.: Late Quaternary  
897 Pollen Records and Climate Significance in Guangzhou, *Acta Scientiarum Naturalium*  
898 *Universitatis Sunyatseni*, 3, 113-121, 2010 (in Chinese with English abstract).

899 Wang, X., Zhang, G., Li, W., Zhang, X., Zhang, E., and Xiao, X.: Environmental changes  
900 during early-middle Holocene from the sediment record of the Chaohu Lake, Anhui  
901 Province, *Chinese Science Bulletin*, 53, 153-160, 2008.

902 Wang, Y., Wang, S., Jiang, F., and Tong, G.: Palynological records in Xipu section,  
903 Yangyuan, *Journal of Geomechanics*, 2, 171-175, 2003 (in Chinese with English abstract).

904 Wang, Y., Wang, S., Zhao, Z., Qin, Y., Ma, Y., Sun, J., Sun, H., and Tian, M.: Vegetation and  
905 Environmental Changes in Hexiqten Qi of Inner Mongolia in the Past 16000 Years, *Acta*  
906 *Geoscientica Sinica*, 5, 449-453, 2005 (in Chinese with English abstract).

907 Wang, Y., Zhao, Z., Qiao, Y., Wang, S., Li, C., and Song, L.: Paleoclimatic and  
908 paleoenvironmental evolution since the late glacial epoch as recorded by sporopollen from  
909 the Hongyuan peat section on the Zoigê Plateau, northern Sichuan, China, *Geological*  
910 *Bulletin of China*, 7, 827-832, 2006 (in Chinese with English abstract).

911 Watanabe, S., Hajima, T., Sudo, K., Nagashima, T., Takemura, T., Okajima, H., Nozawa, T.,  
912 Kawase, H., Abe, M., Yokohata, T., Ise, T., Sato, H., Kato, E., Takata, K., Emori, S., and  
913 Kawamiya, M.: MIROC-ESM 2010: model description and basic results of  
914 CMIP5-20c3m experiments, *Geoscientific Model Development*, 4, 845-872, 2011.

915 Webb, III. T.: Global paleoclimatic data base for 6000 yr BP, Brown Univ., Providence, RI  
916 (USA). Dept. of Geological Sciences, DOE/EV/10097-6; Other: ON: DE85006628 United  
917 States Other: ON: DE85006628 NTIS, PC A08/MF A01. HEDB English, 1985.

- 918 Wen, R., Xiao, J., Chang, Z., Zhai, D., Xu, Q., Li, Y. and Itoh, S.: Holocene precipitation and  
919 temperature variations in the East Asian monsoonal margin from pollen data from Hulun  
920 Lake in northeastern Inner Mongolia, China, *Boreas*, 39, 262-272, 2010.
- 921 Weninger, B., Jöris, O., Danzeglocke, U.: CalPal-2007, Cologne Radiocarbon Calibration and  
922 Palaeoclimate Research Package, <http://www.calpal.de/>, 2007.
- 923 Wischnewski, J., Mischke, S., Wang, Y., and Herzschuh, U.: Reconstructing climate  
924 variability on the northeastern Tibetan Plateau since the last Lateglacial – a multi-proxy,  
925 dual-site approach comparing terrestrial and aquatic signals, *Quaternary Science Reviews*,  
926 30, 82-97, 2011.
- 927 Wohlfahrt, J., Harrison, S. P., and Braconnot, P.: Synergistic feedbacks between ocean and  
928 vegetation on mid- and high-latitude climates during the mid-Holocene, *Climate Dynamics*,  
929 22, 223-238, 2004.
- 930 Wu, H., Guiot, J., Brewer, S., and Guo, Z.: Climatic changes in Eurasia and Africa at the last  
931 glacial maximum and mid-Holocene: reconstruction from pollen data using inverse  
932 vegetation modeling, *Climate Dynamics*, 29, 211-229, 2007.
- 933 Wu, H., Luo, Y., Jiang, W., Li, Q., Sun, A., and Guo, Z.: Paleoclimate reconstruction from  
934 pollen data using inverse vegetation approach: Validation of model using modern data,  
935 *Quaternary Sciences*, 36, 520-529, 2016 (in Chinese with English abstract).
- 936 Wu, H., Ma, Y., Feng, Z., Sun, A., Zhang, C., Li, F., and Kuang, J.: A high resolution record  
937 of vegetation and environmental variation through the last ~25,000 years in the western  
938 part of the Chinese Loess Plateau, *Palaeogeography, Palaeoclimatology, Palaeoecology*,  
939 273, 191-199, 2009.



940 Xia, Y.: Preliminary study on vegetational development and climatic changes in the Sanjiang  
941 Plain in the last 12000 years, *Scientia Geographica Sinica*, 8, 241-249, 1988 (in Chinese  
942 with English abstract).

943 Xia, Z., Chen, G., Zheng, G., Chen, F., and Han, J.: Climate background of the evolution from  
944 Paleolithic to Neolithic cultural transition during the last deglaciation in the middle  
945 reaches of the Yellow River, *Chinese Science Bulletin*, 47, 71-75, 2002.

946 Xiao, J., Lv, H., Zhou, W., Zhao, Z., and Hao, R.: Pollen Vegetation and Environmental  
947 Evolution of the Great Lakes in Jiangxi Province since the Last Glacial Maximum,  
948 *Science in China Series D: Earth Sciences*, 6, 789-797, 2007 (in Chinese with English  
949 abstract).

950 Xiao, J., Xu, Q., Nakamura, T., Yang, X., Liang, W., and Inouchi, Y.: Holocene vegetation  
951 variation in the Daihai Lake region of north-central China: a direct indication of the Asian  
952 monsoon climatic history, *Quaternary Science Reviews*, 23, 1669-1679, 2004.

953 Xiao, X., Haberle, S. G., Shen, J., Yang, X., Han, Y., Zhang, E., and Wang, S.: Latest  
954 Pleistocene and Holocene vegetation and climate history inferred from an alpine  
955 lacustrine record, northwestern Yunnan Province, southwestern China, *Quaternary  
956 Science reviews*, 86, 35-48, 2014.

957 Xie, Y., Li, C., Wang, Q., and Yin, H.: Climatic Change since 9 ka B. P.: Evidence from  
958 Jiangling Area, Jiangnan Plain, China, *Scientia Geographica Sinica*, 2, 199-204, 2006 (in  
959 Chinese with English abstract).

960 Xin, X., Wu, T., and Zhang, J.: Introduction of CMIP5 experiments carried out with the  
961 climate system models of Beijing climate Center, *Advances in Climate Change Research*,  
962 4, 41-49, 2013.

- 963 Xu, J.: Analysis of the Holocene Loess Pollen in Xifeng Area and its Vegetation Evolution,  
964 Capital Normal University, Master Dissertation, 2006 (in Chinese with English abstract).
- 965 Xu, Q., Chen, S., Kong, Z., and Du, N.: Preliminary discussion of vegetation succession and  
966 climate change since the Holocene in the Baiyangdian Lake district, *Acta Phytocologica*  
967 and *Geobotanica Sinica*, 2, 65-73, 1988 (in Chinese with English abstract).
- 968 Xu, Q., Yang, Z., Cui, Z., Yang, X., and Liang.: A Study on Pollen Analysis of Qiguoshan  
969 Section and Ancestor Living Environment in Chifeng Area, Nei Mongol, *Scientia*  
970 *Geographica Sinica*, 4, 453-456, 2002 (in Chinese with English abstract).
- 971 Xu, Y.: The assemblage of Holocene spore pollen and its environment in Bosten Lake area  
972 Xinjiang, *Arid land Geography*, 2, 43-49, 1998 (in Chinese with English abstract).
- 973 Xue, S., and Li, X.: Holocene vegetation characteristics of the southern Loess Plateau in the  
974 Weihe River valley in China, *Review of Palaeobotany & Palynology*, 160 46-52, 2010.
- 975 Yang, J., Cui, Z., Yi, Zhao., Zhang, W., and Liu, K.: Glacial Lacustrine Sediment's Response  
976 to Climate Change since Holocene in Diancang Mountain, *Acta Geographica Sinica*, 4,  
977 525-533, 2004 (in Chinese with English abstract).
- 978 Yang, X., Wang, S., and Tong, G.: Character of analogy and changes of monsoon climate  
979 over the last 10000 years in Gucheng Lake, Jiangsu province, *Journal of Integrative Plant*  
980 *Biology*, 7, 576-581, 1996 (in Chinese with English abstract).
- 981 Yang, Y., and Wang, S.: Study on mire development and paleoenvironment change since  
982 8.0ka B.P. in the northern part of the Sangjiang Plain, *Scientia Geographica Sinica*, 23,  
983 32-38, 2003 (in Chinese with English abstract).

- 984 Yang, Z.: Reconstruction of climate and environment since the Holocene in Diaojiaohaizi  
985 Lake Area, Daqing Mountains, Inner Mongolia, *Acta Ecologica Sinica*, 4, 538-543, 2001  
986 (in Chinese with English abstract).
- 987 Yu, L., Wang, N., Cheng, H., Long, H., and Zhao, Q.: Holocene environmental change in the  
988 marginal area of the Asian monsoon: a record from Zhuye Lake, NW china, *Boreas*, 38,  
989 349-361, 2009.
- 990 Yukimoto, S., Adachi, Y., Hosaka, M., Sakami, T., Yoshimura, H., Hirabara, M., Tanaka,  
991 T.Y., Shindo, E., Tsujino, H., Deushi, M., Mizuta, R., Yabu, S., Obata, A., Nakano, H.,  
992 Koshiro, T., Ose, T., and Kitoh, A.: A new global climate model of the meteorological  
993 research institute: MRI-CGCM3-model description and basic performance, *Journal of the*  
994 *Meteorological Society of Japan*, 90A, 23-64, 2012.
- 995 Zhang, W., Mu, K., Cui, Z., Feng, J., and Yang, J.: Record of the environmental change since  
996 Holocene in the region of Gongwang mountain, Yunan Province, *Earth and Environment*,  
997 4, 343-350, 2007 (in Chinese with English abstract).
- 998 Zhang, Y. G., Pagani, M., and Liu, Z.: A 12-Million-Year Temperature History of the tropical  
999 Pacific Ocean, *Science*, 344, 84-87, 2014.
- 1000 Zhang, Y., and Yu, S.: Palynological assemblages of late Quaternary from the Shenzhen  
1001 region and its paleoenvironment evolution, *Marine Geology & Quaternary Geology*, 2,  
1002 109-114, 1999 (in Chinese with English abstract).
- 1003 Zhang, Y., Jia, L., and Lyu, B.: Studies on Evolution of Vegetation and Climate since 7000  
1004 Years ago in Estuary of Changjiang River Region, *Marine Science Bulletin*, 3, 27-34,  
1005 2004 (in Chinese with English abstract).

- 1006 Zhang, Y., Song, M., and Welker, J. M.: Simulating Alpine Tundra Vegetation Dynamics in  
1007 Response to Global Warming in China, *Global Warming*, Stuart Arthur Harris (Ed.),  
1008 ISBN: 978-953-307-149-7, InTech, 11, 221-250, 2010.
- 1009 Zhang, Z., Xu, Q., Li, Y., Yang, X., Jin, Z., and Tang, J.: Environmental changes of the Yin  
1010 ruins area based on pollen analysis, *Quaternary Science*, 27, 461-468, 2007 (in Chinese  
1011 with English abstract).
- 1012 Zhao, J., Hou, Y., Du, J., and Chen, Y.: Holocene environmental changes in the Guanzhong  
1013 Plain, *Arid Land Geography*, 1, 17-22, 2003 (in Chinese with English abstract).
- 1014 Zhao, Y., Yu, Z., Chen, F., Ito, E., and Zhao, C.: Holocene vegetation and climate history at  
1015 Hurleg Lake in the Qaidam Basin, northwest China, *Review of Palaeobotany and*  
1016 *palynology*, 145, 275-288, 2007.
- 1017 Zheng, R., Xu, X., Zhu, J., Ji, F., Huang, Z., Li, J.: Division of late Quaternary strata and  
1018 analysis of palaeoenvironment in Fuzhou Basin, *Seismology and Geology*, 4, 503-513,  
1019 2002 (in Chinese with English abstract).
- 1020 Zheng, X., Zhang, H., Ming, Q., Chang, F., Meng, H., Zhang, W., Liu, M., Shen, C.:  
1021 Vegetational and environmental changes since 15ka B.P. recorded by lake Lugu in the  
1022 southwest monsoon domain region, *Quaternary Sciences*, 6, 1314-1326, 2014 (in Chinese  
1023 with English abstract).
- 1024 Zhou, J., Liu, D., Zhuang, Z., Wang, Z., and Liu, L.: The sediment layers and the records of  
1025 the Paleoenvironment in the Chaoyanggang Lagoon, Rongcheng City of Shandong  
1026 Province Since Holocene Transgression, *Periodical of Ocean University of China*, 38,  
1027 803-808, 2008 (in Chinese with English abstract).

1028 Zhu, C., Ma, C., Zhang, W., Zheng, C., Tan, L., Lu, X., Liu, K., and Chen, H.: Pollenrecord  
1029 from Dajiuhu Basin of Shennongjia and environmental changes since 15.753 ka B.P.,  
1030 Quaternary Sciences, 5, 814-826, 2006 (in Chinese with English abstract).

1031 Zou, S., Cheng, G., Xiao, H., Xu, B., and Feng, Z.: Holocene natural rhythms of vegetation  
1032 and present potential ecology in the western Chinese Loess Plateau, Quaternary  
1033 International, 194, 55-67, 2009.

1034

1035

1036

1037

1038

1039

1040

1041

1042

1043

1044

1045

1046

1047

1048

**Table 1. Basic information of the pollen dataset used in this study**

<b>Site</b>	<b>Lat</b>	<b>Lon</b>	<b>Alt</b>	<b>Webb 1-7</b>	<b>Source</b>
<b>Sujiawan</b>	35.54	104.52	1700	2	original data (Zou et al., 2009)
<b>Xiaogou</b>	36.10	104.90	1750	2	original data (Wu et al., 2009)
<b>Dadiwan</b>	35.01	105.91	1400	1	original data (Zou et al., 2009)
<b>Sanjiaocheng</b>	39.01	103.34	1320	1	Chen et al., 2006
<b>Chadianpo</b>	36.10	114.40	65	2	Zhang et al., 2007
<b>Qindeli</b>	48.08	133.25	60	2	Yang and Wang, 2003
<b>Fuyuanchuangye</b>	47.35	133.03	56	3	Xia, 1988
<b>Jingbo Lake</b>	43.83	128.50	350	2	Li et al., 2011
<b>Hani Lake</b>	42.22	126.52	900	1	Cui et al., 2006
<b>Jinchuan</b>	42.37	126.43	662	5	Jiang et al., 2008
<b>Maar Lake</b>	42.30	126.37	724	1	Liu et al., 2009
<b>Maar Lake</b>	42.30	126.37	724	1	Liu et al., 2008
<b>Xie Lake SO4</b>	37.38	122.52	0	1	Zhou et al., 2008
<b>Nanhuiheming Core</b>	31.05	121.58	7	2	Jia and Zhang, 2006
<b>Toushe</b>	23.82	120.88	650	1	Liu et al., 2006
<b>Dongyuan Lake</b>	22.17	120.83	415	2	Lee et al., 2010
<b>Yonglong CY</b>	31.78	120.44	5	3	Zhang et al., 2004
<b>Hangzhou HZ3</b>	30.30	120.33	6	4	Liu et al., 2007
<b>Xinhua XH1</b>	32.93	119.83	2	3	Shu et al., 2008
<b>ZK01</b>	31.77	119.80	6	2	Shu et al., 2007
<b>Chifeng</b>	43.97	119.37	503	2	Xu et al., 2002
<b>SZK1</b>	26.08	119.31	9	1	Zheng et al., 2002
<b>Gucheng</b>	31.28	118.90	6	4	Yang et al., 1996
<b>Lulong</b>	39.87	118.87	23	2	Kong et al., 2000
<b>Hulun Lake</b>	48.92	117.42	545	1	Wen et al., 2010
<b>CH-1</b>	31.56	117.39	5	2	Wang et al., 2008
<b>Sanyi profile</b>	43.62	117.38	1598	4	Wang et al., 2005
<b>Xiaoniuchang</b>	42.62	116.82	1411	1	Liu et al., 2002
<b>Haoluku</b>	42.87	116.76	1333	2	Liu et al., 2002
<b>Liuzhouwan</b>	42.71	116.68	1410	7	Liu et al., 2002
<b>Poyang Lake 103B</b>	28.87	116.25	16	4	Jiang and Piperno, 1999
<b>Baiyangdian</b>	38.92	115.84	8	2	Xu et al., 1988
<b>Bayanchagan</b>	42.08	115.35	1355	1	Jiang et al., 2006
<b>Huangjiapu</b>	40.57	115.15	614	7	Sun et al., 2001
<b>Dingnan</b>	24.68	115.00	250	2	Xiao et al., 2007
<b>Guang1</b>	36.02	114.53	56	1	Zhang et al., 2007
<b>Angulinao</b>	41.33	114.35	1315	1	Wang et al., 2010
<b>Yangyuanxipu</b>	40.12	114.22	921	6	Wang et al., 2003

<b>Shenzhen Sx07</b>	22.75	113.78	2	2	Zhang and Yu, 1999
<b>GZ-2</b>	22.71	113.51	1	7	Wang et al., 2010
<b>Daihai99a</b>	40.55	112.66	1221	2	Xiao et al., 2004
<b>Daihai</b>	40.55	112.66	1221	2	Sun et al., 2006
<b>Sihenan profile</b>	34.80	112.40	251	1	Sun and Xia, 2005
<b>Diaojiaohaizi</b>	41.30	112.35	2015	1	Yang et al., 2001
<b>Ganhaizi</b>	39.00	112.30	1854	3	Meng et al., 2007
<b>Jiangling profile</b>	30.35	112.18	37	1	Xie et al., 2006
<b>Helingeer</b>	40.38	111.82	1162	3	Li et al., 2011
<b>Shennongjia2</b>	31.75	110.67	1700	1	Liu et al., 2001
<b>Huguangyan Maar Lake B</b>	21.15	110.28	59	2	Wang et al., 2007
<b>Yaoxian</b>	35.93	110.17	1556	2	Li et al., 2003
<b>Jixian</b>	36.00	110.06	1005	6	Xia et al., 2002
<b>Shennongjia Dajiu Lake</b>	31.49	110.00	1760	2	Zhu et al., 2006
<b>Qigai nuur</b>	39.50	109.85	1300	1	Sun and Feng, 2013
<b>Beizhuangcun</b>	34.35	109.53	519	1	Xue et al., 2010
<b>Lantian</b>	34.15	109.33	523	1	Li and Sun, 2005
<b>Bahanniao</b>	39.32	109.27	1278	1	Guo et al., 2007
<b>Midiwan</b>	37.65	108.62	1400	1	Li et al., 2003
<b>Jinbian</b>	37.50	108.33	1688	2	Cheng, 2011
<b>Xindian</b>	34.38	107.80	608	1	Xue et al., 2010
<b>Nanguanzhuang</b>	34.43	107.75	702	1	Zhao et al., 2003
<b>Xifeng</b>	35.65	107.68	1400	3	Xu, 2006
<b>Jiyuan</b>	37.13	107.40	1765	3	Li et al., 2011
<b>Jiacunyuan</b>	34.27	106.97	1497	2	Gong, 2006
<b>Dadiwan</b>	35.01	105.91	1400	1	Zou et al., 2009
<b>Maying</b>	35.34	104.99	1800	1	Tang and An, 2007
<b>Huiningxiaogou</b>	36.10	104.90	1750	2	Wu et al., 2009
<b>Sujiawan</b>	35.54	104.52	1700	2	Zou et al., 2009
<b>QTH02</b>	39.07	103.61	1302	1	Yu et al., 2009
<b>Laotanfang</b>	26.10	103.20	3579	2	Zhang et al., 2007
<b>Hongshui River2</b>	38.17	102.76	1511	1	Ma et al., 2003,
<b>Ruoergai</b>	33.77	102.55	3480	1	Cai, 2008
<b>Hongyuan</b>	32.78	102.52	3500	2	Wang et al., 2006
<b>Dahaizi</b>	27.50	102.33	3660	1	Li et al., 1988
<b>Shayema Lake</b>	28.58	102.22	2453	1	Tang and Shen, 1996
<b>Luanhaizi</b>	37.59	101.35	3200	5	Herzschuh et al., 2006
<b>Lugu Lake</b>	27.68	100.80	2692	1	Zheng et al., 2014
<b>Qinghai Lake</b>	36.93	100.73	3200	2	Shen et al., 2004
<b>Dalianhai</b>	36.25	100.41	2850	3	Cheng et al., 2010
<b>Erhai ES Core</b>	25.78	100.19	1974	1	Shen et al., 2006
<b>Xianmachi profile</b>	25.97	99.87	3820	7	Yang et al., 2004

<b>TCK1</b>	26.63	99.72	3898	1	Xiao et al., 2014
<b>Yidun Lake</b>	30.30	99.55	4470	4	Shen et al., 2006
<b>Kuhai lake</b>	35.30	99.20	4150	1	Wischniewski et al., 2011
<b>Koucha lake</b>	34.00	97.20	4540	2	Herzschuh et al., 2009
<b>Hurleg</b>	37.28	96.90	2817	2	Zhao et al., 2007
<b>Basu</b>	30.72	96.67	4450	3	Tang et al., 1998
<b>Tuolekule</b>	43.34	94.21	1890	1	An et al., 2011
<b>Balikun</b>	43.62	92.77	1575	1	Tao et al., 2010
<b>Cuona</b>	31.47	91.51	4515	3	Tang et al., 2009
<b>Dongdaohaizi2</b>	44.64	87.58	402	1	Li et al., 2001
<b>Bositeng Lake</b>	41.96	87.21	1050	1	Xu, 1998
<b>Cuoqin</b>	31.00	85.00	4648	4	Luo, 2008
<b>Yili</b>	43.86	81.97	928	2	Li et al., 2011
<b>Bangong Lake</b>	33.75	78.67	4241	1	Huang et al., 1996
<b>Shengli</b>	47.53	133.87	52	2	CQPD, 2000
<b>Qingdeli</b>	48.05	133.17	52	1	CQPD, 2000
<b>Changbaishan</b>	42.22	126.00	500	2	CQPD, 2000
<b>Liuhe</b>	42.90	125.75	910	7	CQPD, 2000
<b>Shuangyang</b>	43.27	125.75	215	1	CQPD, 2000
<b>Xiaonan</b>	43.33	125.33	209	1	CQPD, 2000
<b>Tailai</b>	46.40	123.43	146	5	CQPD, 2000
<b>Sheli</b>	45.23	123.31	150	4	CQPD, 2000
<b>Tongtu</b>	45.23	123.30	150	7	CQPD, 2000
<b>Yueyawan</b>	37.98	120.71	5	1	CQPD, 2000
<b>Beiwangxu</b>	37.75	120.61	6	1	CQPD, 2000
<b>East Tai Lake1</b>	31.30	120.60	3	1	CQPD, 2000
<b>Suzhou</b>	31.30	120.60	2	7	CQPD, 2000
<b>Sun-Moon Lake</b>	23.51	120.54	726	2	CQPD, 2000
<b>West Tai Lake</b>	31.30	119.80	1	1	CQPD, 2000
<b>Changzhou</b>	31.43	119.41	5	1	CQPD, 2000
<b>Dazeyin</b>	39.50	119.17	50	7	CQPD, 2000
<b>Hailaer</b>	49.17	119.00	760	2	CQPD, 2000
<b>Cangumiao</b>	39.97	118.60	70	1	CQPD, 2000
<b>Qianhuzhuang</b>	40.00	118.58	80	6	CQPD, 2000
<b>Reshuitang</b>	43.75	117.65	1200	1	CQPD, 2000
<b>Yangerzhuang</b>	38.20	117.30	5	7	CQPD, 2000
<b>Mengcun</b>	38.00	117.06	7	5	CQPD, 2000
<b>Hanjiang-CH2</b>	23.48	116.80	5	2	CQPD, 2000
<b>Hanjiang-SH6</b>	23.42	116.68	3	7	CQPD, 2000
<b>Hanjiang-SH5</b>	23.45	116.67	8	2	CQPD, 2000
<b>Hulun Lake</b>	48.90	116.50	650	1	CQPD, 2000
<b>Heitutang</b>	40.38	113.74	1060	1	CQPD, 2000
<b>Zhujiang delta PK16</b>	22.73	113.72	15	7	CQPD, 2000



<b>Angulitun</b>	41.30	113.70	1400	7	CQPD, 2000
<b>Bataigou</b>	40.92	113.63	1357	1	CQPD, 2000
<b>Dahewan</b>	40.87	113.57	1298	2	CQPD, 2000
<b>Yutubao</b>	40.75	112.67	1254	7	CQPD, 2000
<b>Zhujiang delta K5</b>	22.78	112.63	12	1	CQPD, 2000
<b>Da-7</b>	40.52	112.62	1200	3	CQPD, 2000
<b>Hahai-1</b>	40.17	112.50	1200	5	CQPD, 2000
<b>Wajianggou</b>	40.50	112.50	1476	4	CQPD, 2000
<b>Shuidong Core A1</b>	21.75	111.07	-8	2	CQPD, 2000
<b>Dajahu</b>	31.50	110.33	1700	2	CQPD, 2000
<b>Tianshuigou</b>	34.87	109.73	360	7	CQPD, 2000
<b>Mengjiawan</b>	38.60	109.67	1190	7	CQPD, 2000
<b>Fuping BK13</b>	34.70	109.25	422	7	CQPD, 2000
<b>Yaocun</b>	34.70	109.22	405	2	CQPD, 2000
<b>Jinbian</b>	37.80	108.60	1400	4	CQPD, 2000
<b>Dishaogou</b>	37.83	108.45	1200	2	CQPD, 2000
<b>Shuidonggou</b>	38.20	106.57	1200	5	CQPD, 2000
<b>Jiuzhoutai</b>	35.90	104.80	2136	7	CQPD, 2000
<b>Luojishan</b>	27.50	102.40	3800	1	CQPD, 2000
<b>RM-F</b>	33.08	102.35	3400	2	CQPD, 2000
<b>Hongyuan</b>	33.25	101.57	3492	1	CQPD, 2000
<b>Wasong</b>	33.20	101.52	3490	1	CQPD, 2000
<b>Guhu Core 28</b>	27.67	100.83	2780	7	CQPD, 2000
<b>Napahai Core 34</b>	27.80	99.60	3260	2	CQPD, 2000
<b>Lop Nur</b>	40.50	90.25	780	7	CQPD, 2000
<b>Chaiwobao1</b>	43.55	87.78	1100	2	CQPD, 2000
<b>Chaiwobao2</b>	43.33	87.47	1114	1	CQPD, 2000
<b>Manasi</b>	45.97	84.83	257	2	CQPD, 2000
<b>Wuqia</b>	43.20	83.50	1000	7	CQPD, 2000
<b>Madagou</b>	37.00	80.70	1370	2	CQPD, 2000
<b>Tongyu</b>	44.83	123.10	148	5	CQPD, 2000
<b>Nanjing</b>	32.15	119.05	10	2	CQPD, 2000
<b>Banpo</b>	34.27	109.03	395	1	CQPD, 2000
<b>QL-1</b>	34.00	107.58	2200	7	CQPD, 2000
<b>Dalainu</b>	43.20	116.60	1290	7	CQPD, 2000
<b>Qinghai</b>	36.55	99.60	3196	2	CQPD, 2000

1050

1051

1052

1053

1054

1055 **Table 2. Earth's orbital parameters and trace gases as recommended by the PMIP3**  
 1056 **project**

Simulation	Orbital parameters			Trace gases		
	Eccentricity	Obliquity(°)	Angular precession(°)	CO <sub>2</sub> (ppmv)	CH <sub>4</sub> (ppbv)	N <sub>2</sub> O(ppbv)
<b>PI</b>	0,0167724	23,446	102,04	280	760	270
<b>MH</b>	0,018682	24,105	0,87	280	650	270

1057

1058

1059 **Table 3. PMIP3 model characteristics and references**

<i>Model Name</i>	<i>Modelling centre</i>	<i>Type</i>	<i>Grid</i>	<i>Reference</i>
<b>BCC-CSM-1-1</b>	BCC-CMA (China)	AOVGCM	Atm: 128×64×L26; Ocean: 360×232×L40	Xin et al. (2013)
<b>CCSM4</b>	NCAR (USA)	AOGCM	Atm: 288 × 192×L26; Ocean: 320×384×L60	Gent et al. (2011)
<b>CNRM-CM5</b>	CNRM&CERFACS (France)	AOGCM	Atm: 256 × 128×L31; Ocean: 362×292×L42	Voltaire et al. (2012)
<b>CSIRO-Mk3-6-0</b>	QCCCE, Australia	AOGCM	Atm: 192 × 96×L18; Ocean: 192×192×L31	Jeffrey et al. (2013)
<b>FGOALS-g2</b>	LASG-IAP (China)	AOVGCM	Atm: 128 × 60×L26; Ocean: 360×180×L30	Li et al. (2013)
<b>FGOALS-s2</b>	LASG-IAP (China)	AOVGCM	Atm: 128 × 108×L26; Ocean: 360×180×L30	Bao et al. (2013)
<b>GISS-E2-R</b>	GISS (USA)	AOGCM	Atm: 144 × 90×L40; Ocean: 288×180×L32	Schmidt et al. (2014a,b)
<b>HadGEM2-CC</b>	Hadley Centre (UK)	AOVGCM	Atm: 192 × 145×L60; Ocean: 360×216×L40	Collins et al. (2011)
<b>HadGEM2-ES</b>	Hadley Centre (UK)	AOVGCM	Atm: 192 × 145×L38; Ocean: 360×216×L40	Collins et al. (2011)
<b>IPSL-CM5A-LR</b>	IPSL (France)	AOVGCM	Atm: 96 × 96×L39; Ocean: 182×149×L31	Dufresne et al. (2013)
<b>MIROC-ESM</b>	Utokyo&NIES (Japan)	AOVGCM	Atm: 128×64×L80; Ocean: 256×192×L44	Watanabe et al. (2011)
<b>MPI-ESM-P</b>	MPI (Germany)	AOGCM	Atm: 196×98×L47; Ocean: 256×220×L40	Giorgetta et al. (2013)
<b>MRI-CGCM3</b>	MRI (Japan)	AOGCM	Atm: 320 × 160×L48; Ocean: 364×368×L51	Yukimoto et al. (2012)

1060

1061

1062

1063 **Table 4. Important values for each plant life form used in the  $\Delta V$  statistical calculation**  
 1064 **as assigned to the megabiomes**

<i>Megabiomes</i>	<i>Life form</i>		
	<b>Trees</b>	<b>Grass/grass</b>	<b>Bare ground</b>
<i>Tropical forest</i>	1		
<i>Warm mixed forest</i>	1		
<i>Temperate forest</i>	1		
<i>Boreal forest</i>	1		
<i>Grassland and dry shrubland</i>	0.25	0.75	
<i>Savanna and dry woodland</i>	0.5	0.5	
<i>Desert</i>		0.25	0.75
<i>Tundra</i>		0.75	0.25

1065

1066 **Table 5. Attribute values and the weights for plant life forms used by the  $\Delta V$  statistic**

<i>Life form</i>	<i>Attribute</i>			
	<b>Evergreen</b>	<b>Needle-leaf</b>	<b>Tropical</b>	<b>Boreal</b>
<b><i>Trees</i></b>				
<i>Tropical forest</i>	1	0	1	0
<i>Warm mixed forest</i>	0.75	0.25	0	0
<i>Temperate forest</i>	0.5	0.5	0	0.5
<i>Boreal forest</i>	0.25	0.75	0	1
<i>Grassland and dry shrubland</i>	0.75	0.25	0.75	0
<i>Savanna and dry woodland</i>	0.25	0.75	0	0.5
<i>weights</i>	0.2	0.2	0.3	0.3
<b><i>Grass/Shrub</i></b>	<b>Warm</b>	<b>Arctic/alpine</b>		
<i>Grassland and dry shrubland</i>	1	0		
<i>Savanna and dry woodland</i>	0.75	0		
<i>Desert</i>	1	0		
<i>Tundra</i>	0	1		
<i>weights</i>	0.5	0.5		
<b><i>Bare Ground</i></b>	<b>Arctic/alpine</b>			
<i>Desert</i>	0			
<i>Tundra</i>	1			
<i>weight</i>	1			

1067

1068  
1069

**Table 6. Regression coefficients between the reconstructed climates by inverse vegetation models and observed meteorological values**

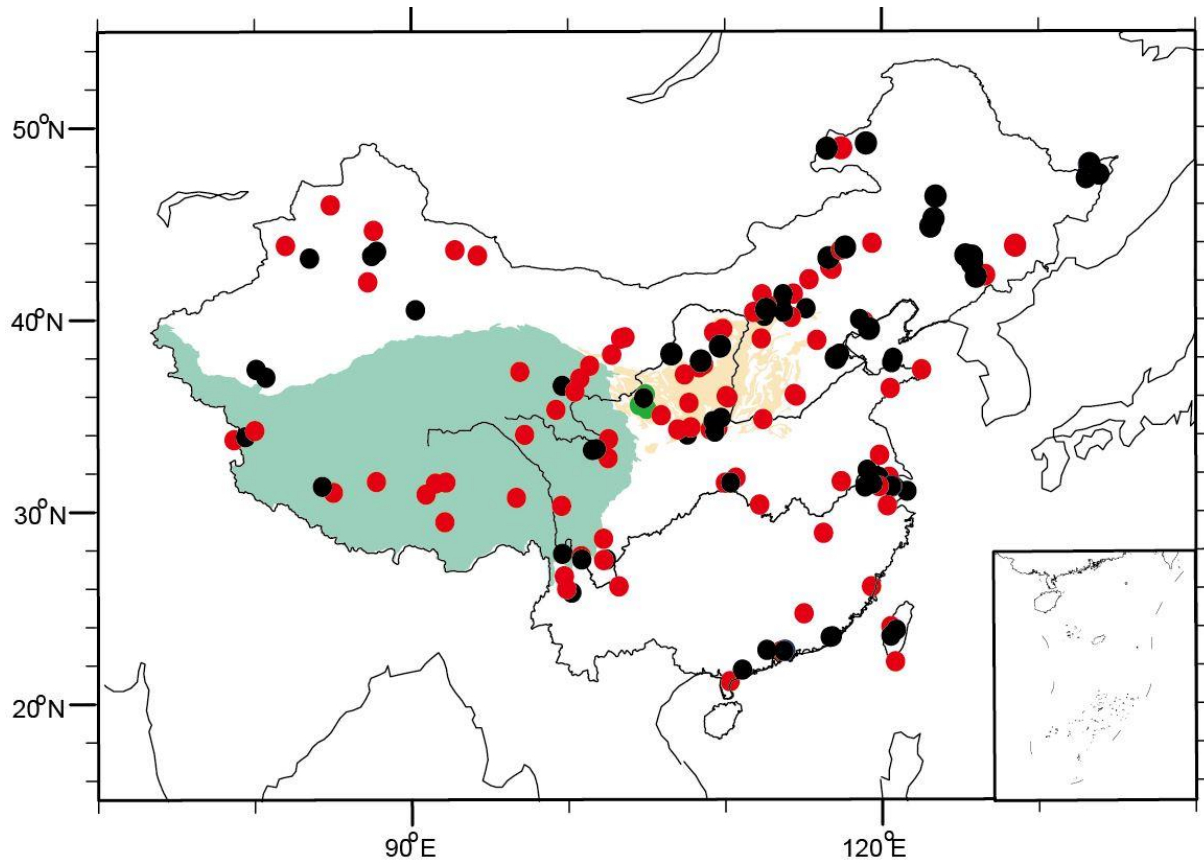
Climate parameter	Slope	Intercept	R	ME	RMSE
<b>MAT</b>	0.82±0.02	0.92±0.18	0.89	0.16	3.25
<b>MTCO</b>	0.81±0.01	-1.79±0.18	0.95	-0.17	3.19
<b>MTWA</b>	0.75±0.03	4.57±0.60	0.75	-0.19	4.02
<b>MAP</b>	1.15±0.02	32.90±18.41	0.94	138.01	263.88
<b>Pjan</b>	1.01±0.02	0.32±0.47	0.94	0.52	8.89
<b>Pjul</b>	1.30±0.03	-21.67±4.52	0.89	16.45	52.9

1070  
1071  
1072  
1073  
1074  
1075

The climatic parameters used for regression are the actual values (data source: China Climate Bureau, China Ground Meteorological Record Monthly Report, 1951-2001). MAT annual mean temperature, MTCO mean temperature of the coldest month, MTWA mean temperature of the warmest month, MAP annual precipitation, RMSE the root-mean-square error of the residuals, ME mean error of the residuals, Pjan: precipitation of January, Pjul: precipitation of July, R is the correlation coefficient, ± stand error

1076  
1077  
1078  
1079  
1080  
1081  
1082  
1083  
1084  
1085  
1086  
1087  
1088  
1089  
1090  
1091  
1092  
1093  
1094

1095  
1096  
1097  
1098



1099

1100 **Figure 1.** Distribution of pollen sites during mid-Holocene period in China. Black circle is the  
1101 original China Quaternary Pollen Database, red circles are digitized ones from published  
1102 papers, green circles represent the three original pollen data used in this study. The area with  
1103 green color represents the Tibetan Plateau, yellow color for the Loess Plateau.

1104  
1105  
1106  
1107  
1108  
1109  
1110  
1111  
1112  
1113

1114  
 1115  
 1116  
 1117  
 1118  
 1119  
 1120  
 1121  
 1122  
 1123  
 1124  
 1125  
 1126  
 1127  
 1128  
 1129  
 1130  
 1131  
 1132  
 1133  
 1134  
 1135  
 1136  
 1137  
 1138  
 1139  
 1140  
 1141  
 1142  
 1143  
 1144  
 1145

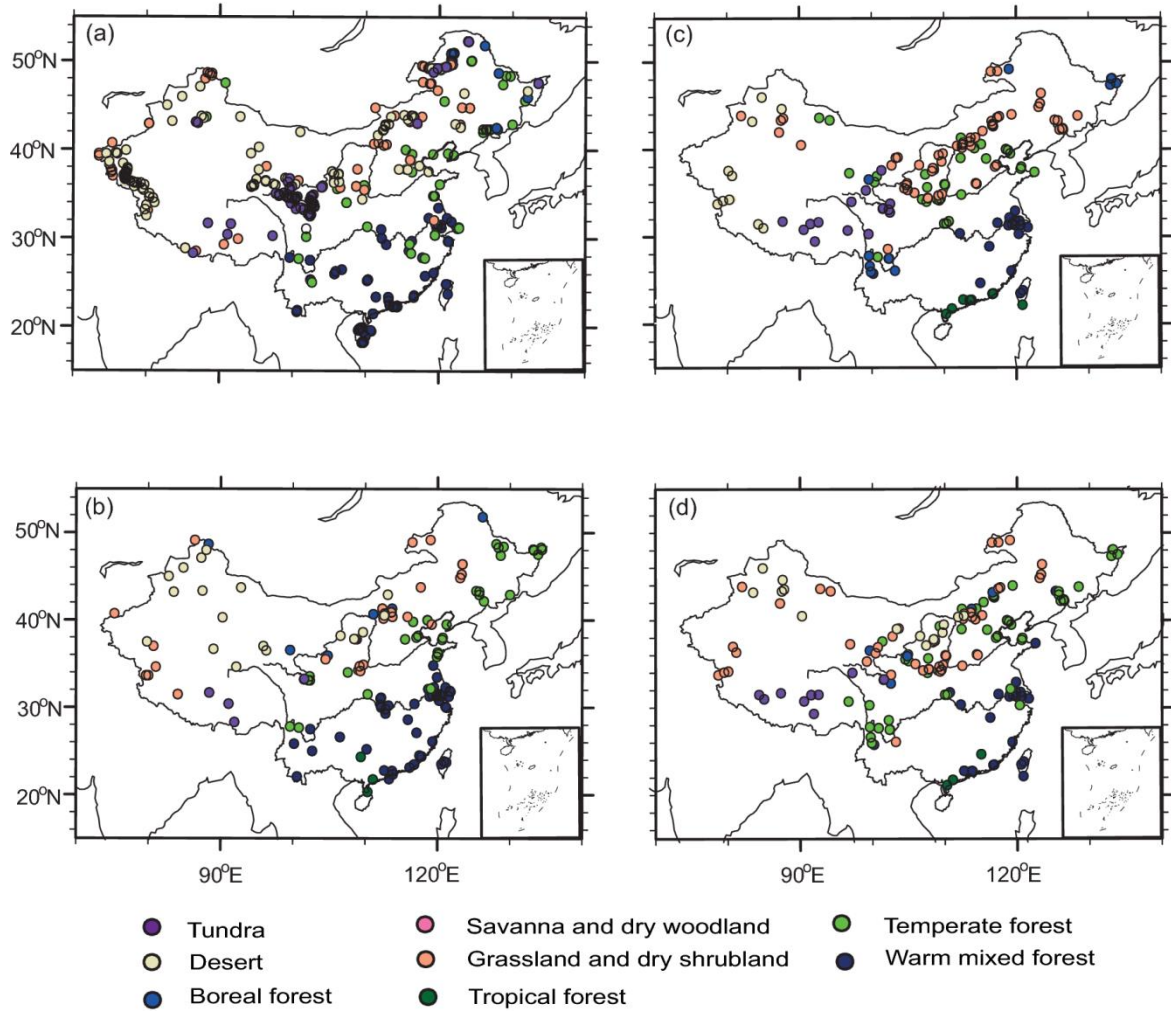
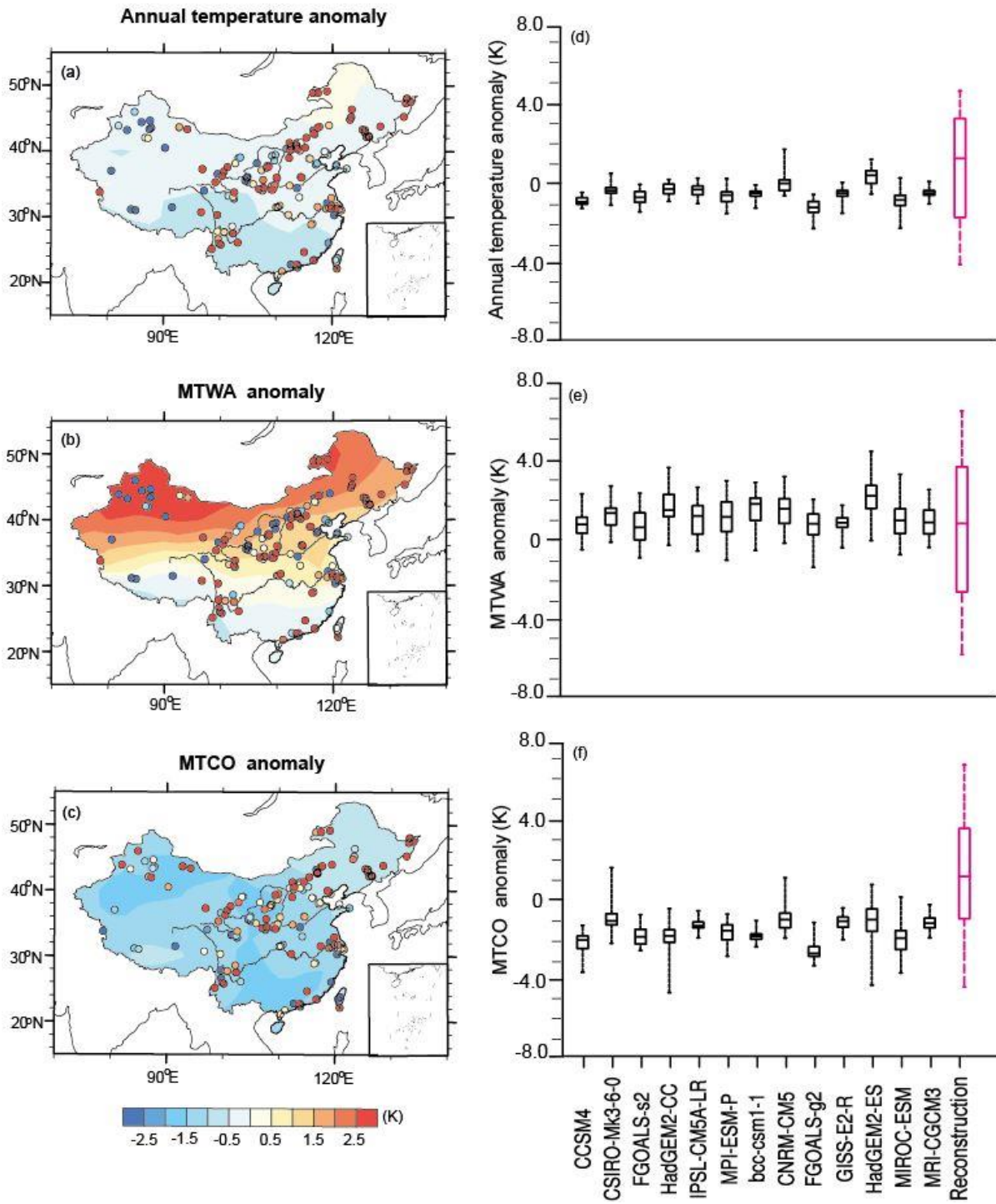


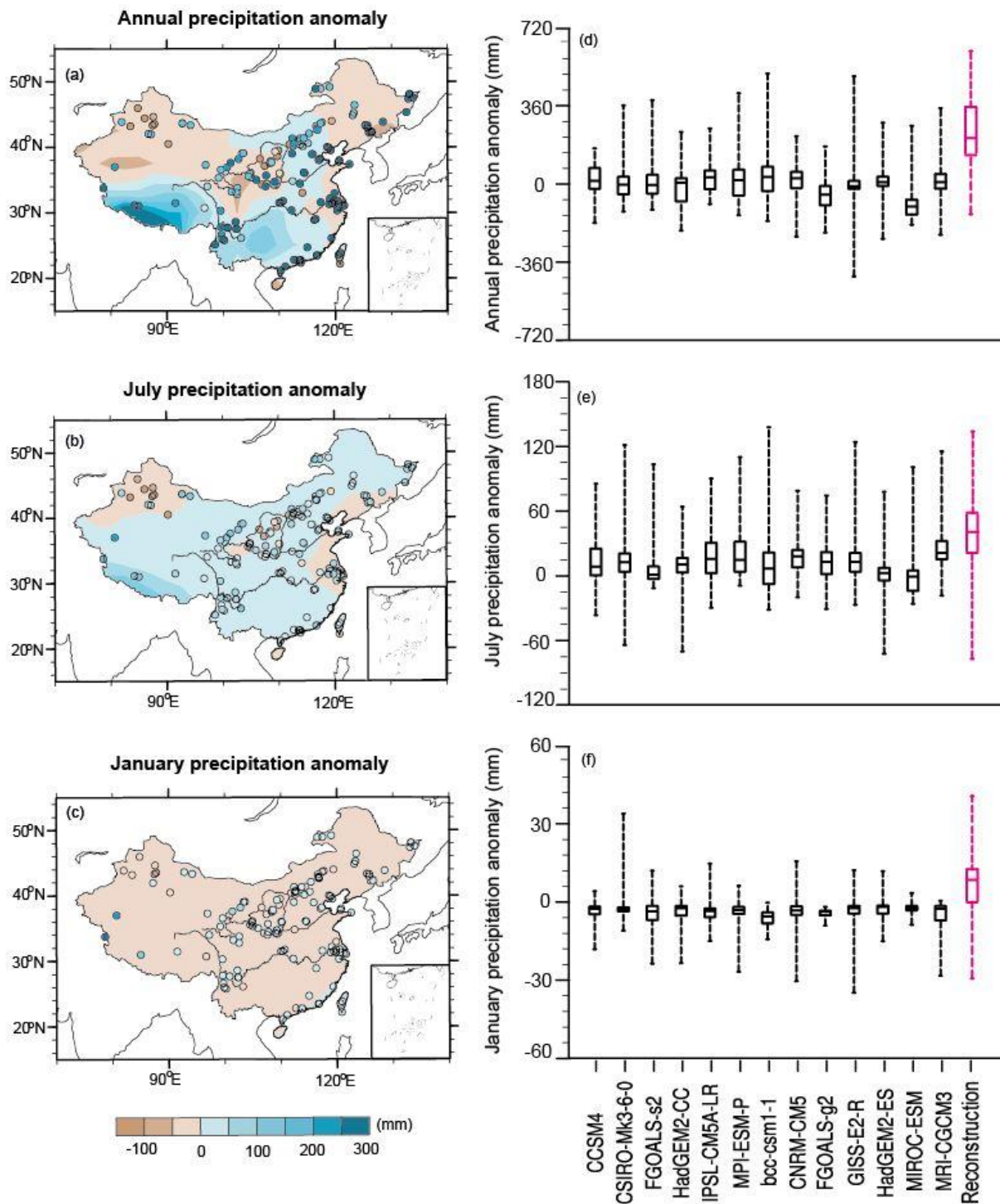
**Figure 2.** Comparison of megabiomes for PI (first row) and the MH (second row): (a,b) BIOME6000, (c,d) pollen data collected in this study.



1147

1148 **Figure 3.** Model-data comparison for annual and seasonal (MTWA and MTCO) temperature  
 1149 (K). For the left panel (a-c), points represent the reconstruction from IVM, shades show the  
 1150 last 30-year means simulation results of multi-model ensemble (MME) for 13 PMIP3 models.  
 1151 The box-and-whisker plots (d-f) show the changes as shown by each PMIP3 model and the  
 1152 reconstruction. (d) considers changes in annual temperature, (e) indicates changes in MTWA,  
 1153 and (f) shows changes in MTCO. The lines in each box shows the median value from each set  
 1154 of measurements, the box shows the 25%-75% range, and the whiskers show the 90% interval  
 1155 (5th to 95th percentile).



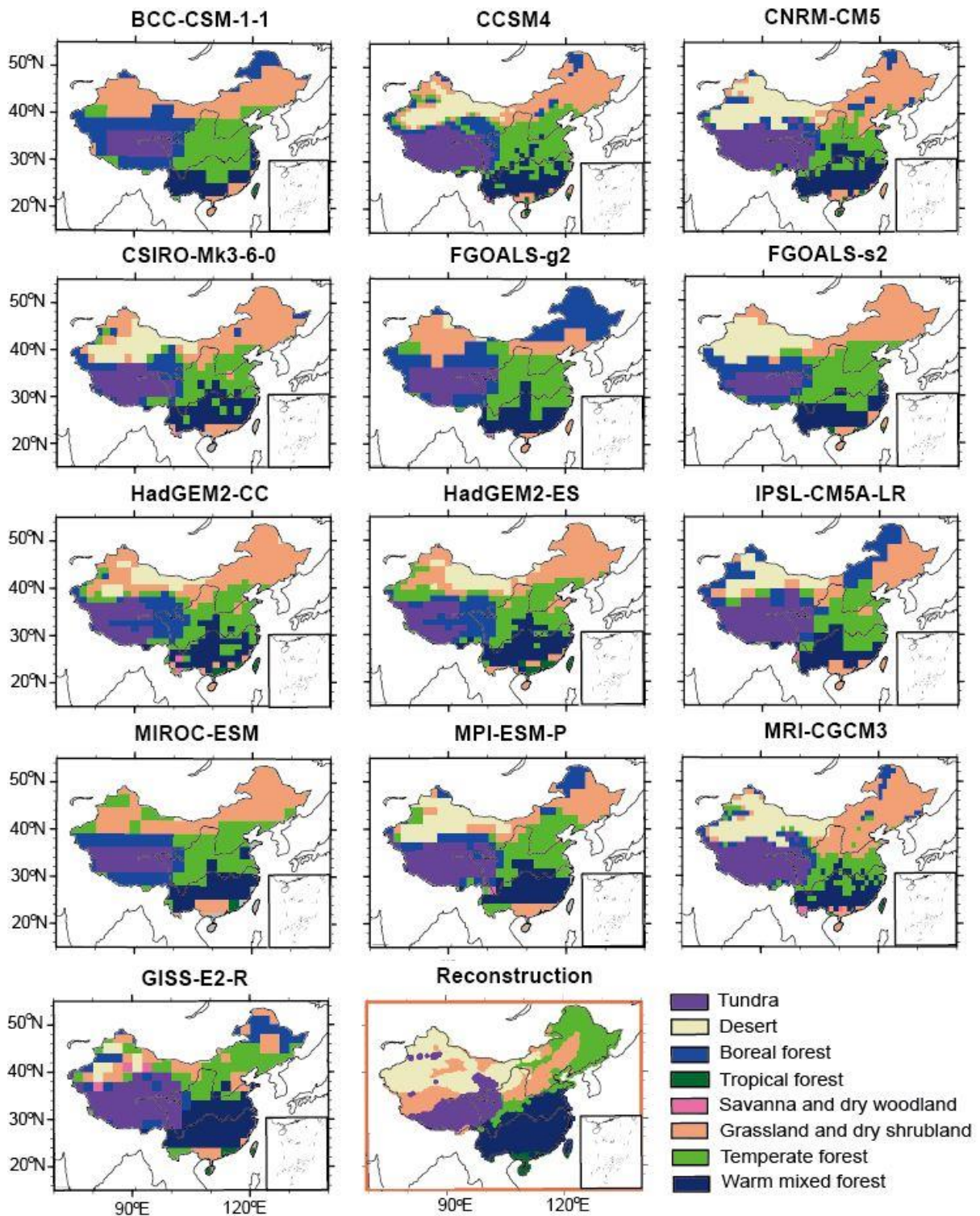


1156

1157 **Figure 4.** Model-data comparison for annual, July and January precipitation (mm). For the  
 1158 left panel (a,b), points represent the reconstruction from IVM, shades show the last 30-year  
 1159 means simulation results of multi-model ensemble (MME) for 13 PMIP3 models. The  
 1160 box-and-whisker plots (d-f) show the changes as shown by each PMIP3 model and the  
 1161 reconstruction. (d) considers changes in annual precipitation, (e) indicates changes in July  
 1162 precipitation, and (f) shows changes in January precipitation. The lines in each box shows the  
 1163 median value from each set of measurements, the box shows the 25%-75% range, and the  
 1164 whiskers show the 90% interval (5th to 95th percentile).

1165





1166

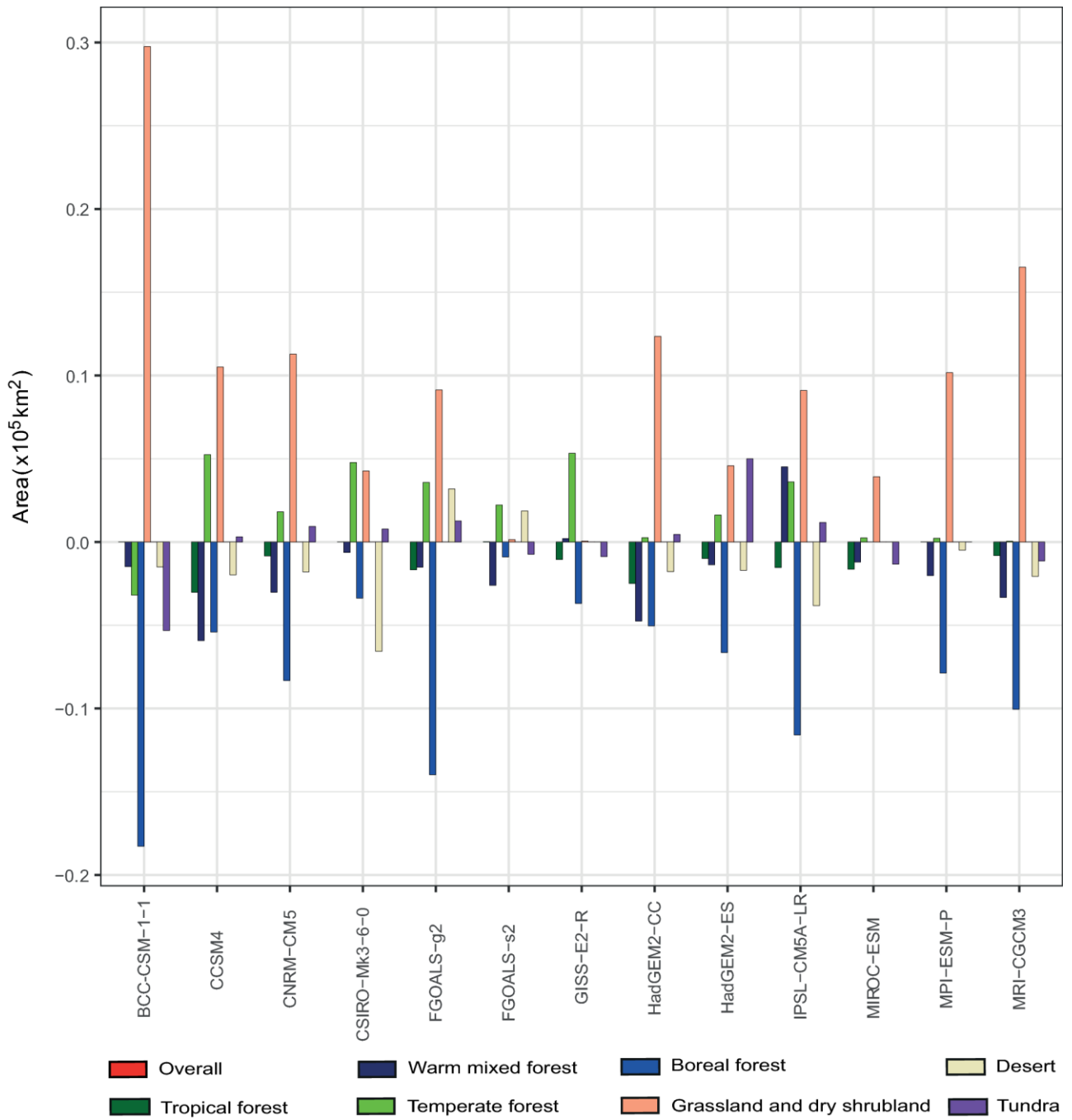
1167 **Figure 5.** Comparison of interpolated megabiomes distribution (plot in red rectangle) with the  
 1168 simulated spatial pattern from BIOME4 for each model during mid-Holocene.

1169

1170

1171

1172



1173

1174 **Figure 6.** Changes in the extent of each megabiome as a consequence of simulated climate  
 1175 changes for each model, both expressed as change relative to the PI extent of same  
 1176 megabiome.

1177

1178

1179

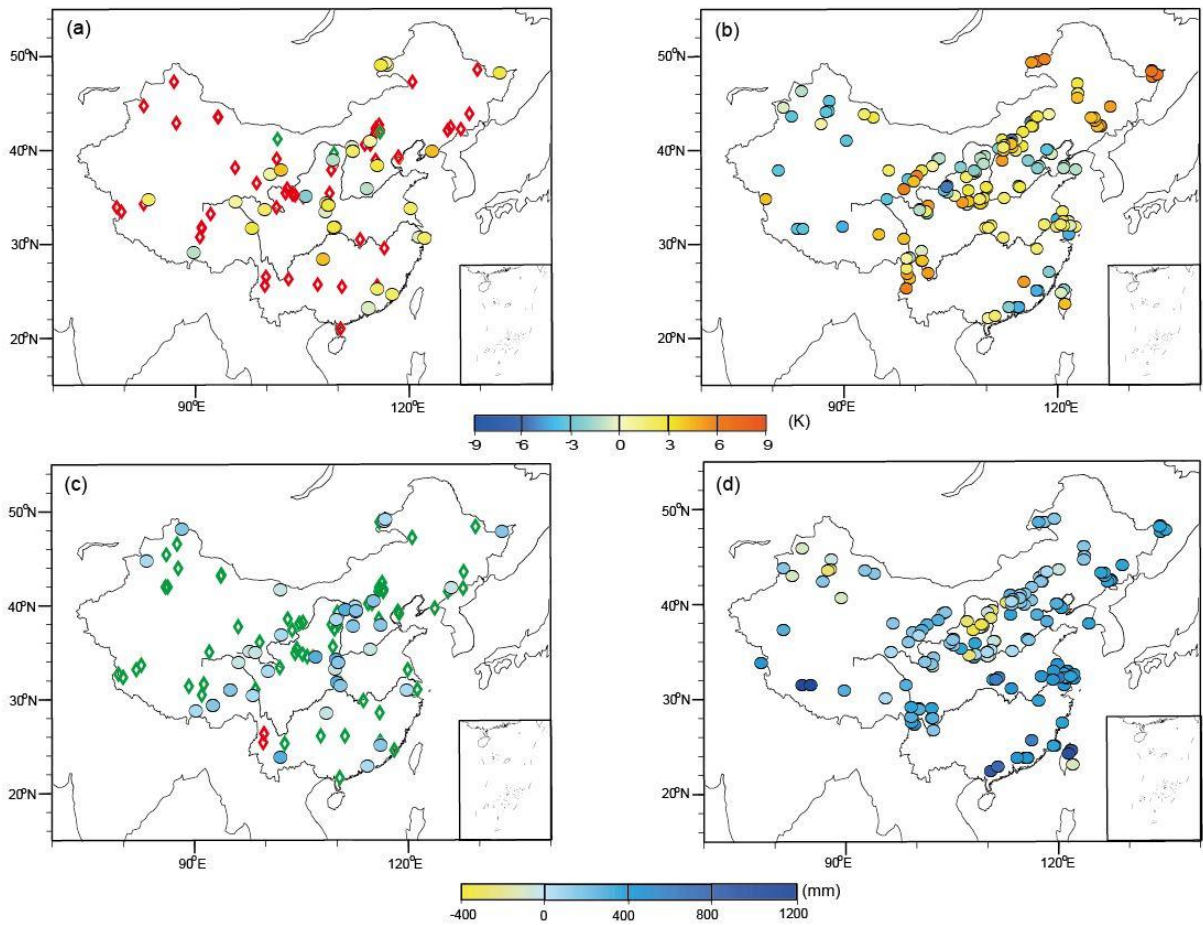
1180

1181

1182

1183

1184



1185

1186

1187 **Figure 7.** Comparison between the climate reconstruction and previous reconstruction over  
1188 China. (a) Previous temperature results. Diamond is the qualitative reconstruction, red is the  
1189 temperature increase and green is the temperature decrease; Circle is quantitative  
1190 reconstruction; (b) Mean annual temperature reconstruction in this study; (c) Previous  
1191 precipitation results, diamond is the qualitative reconstruction, red is the precipitation increase  
1192 and green is the precipitation decrease; Circle is the quantitative reconstruction; (d) Mean  
1193 annual precipitation reconstruction in this study.

1194

1195

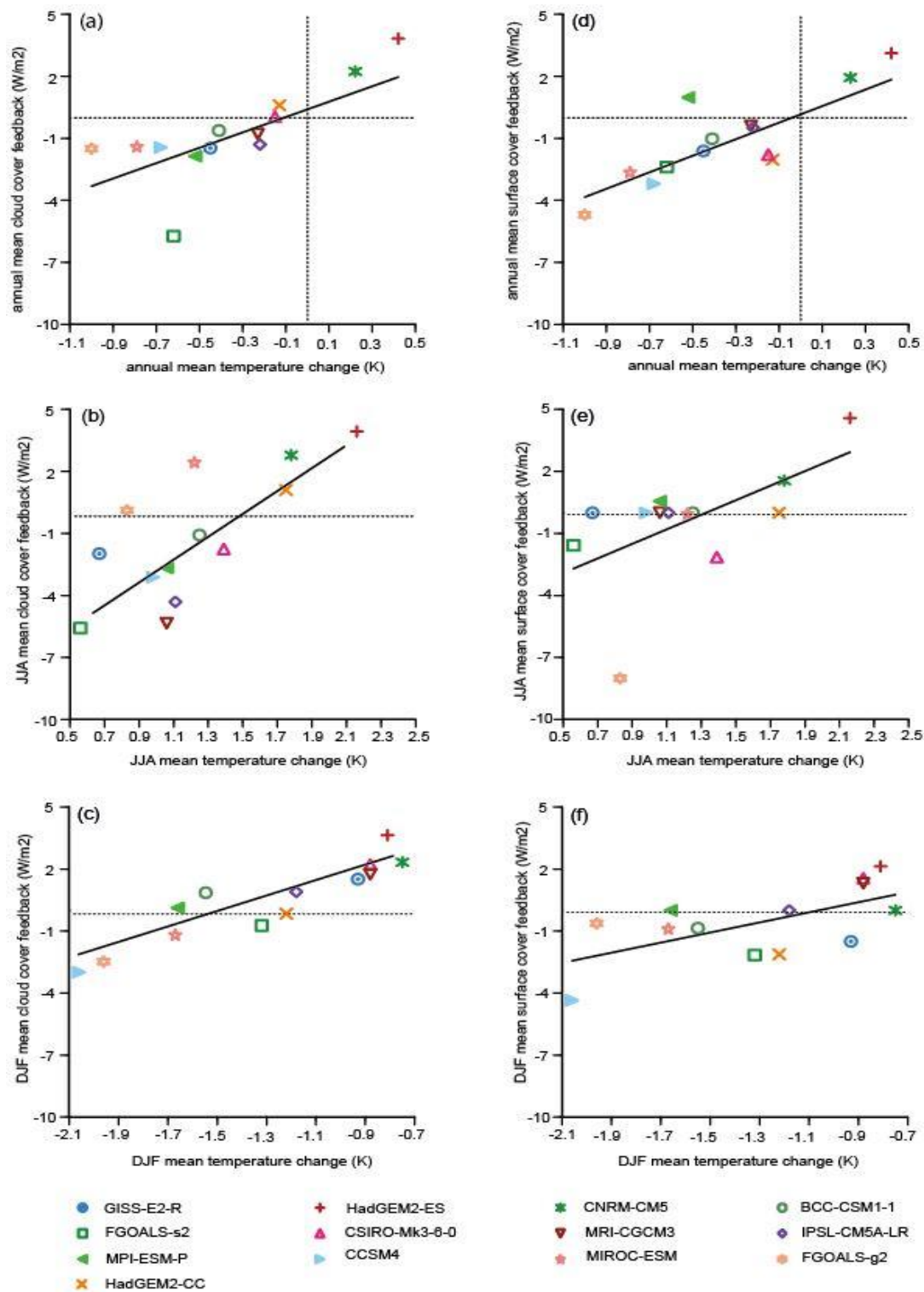
1196

1197

1198

1199

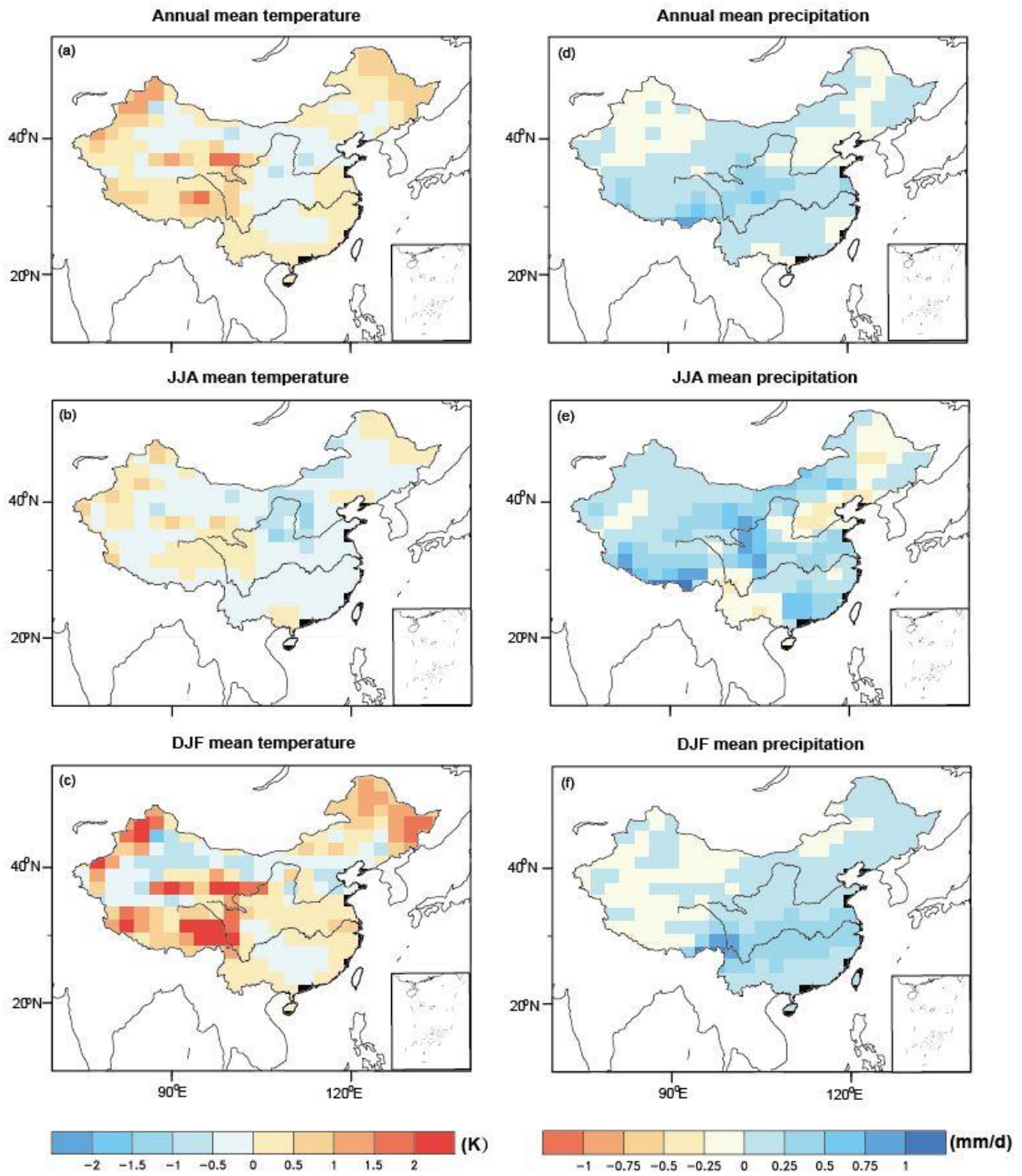
1200



1201

1202 **Figure 8.** Scatter plots showing temperature, cloud cover feedback and surface albedo  
 1203 feedback changes during the MH. The values shown are the simulated 30-year mean anomaly  
 1204 (MH-PI) for the 13 models. **a**, annual mean temperature relative to the annual mean cloud  
 1205 cover feedback and **d**, annual surface albedo feedback. **b**, Summer (JJA) mean temperature  
 1206 relative to the summer mean cloud cover feedback and **e**, Summer surface albedo feedback.  
 1207 **c**, Winter (DJF) mean temperature relative to the summer mean cloud cover feedback and **f**,  
 1208 Winter surface albedo feedback. The horizontal and vertical lines in plots represent the value  
 1209 of 0.





1211

1212 **Figure 9.** Climate anomalies between the two experiments (6 ka and 6 ka\_VEG) conducted in  
1213 CESM version 1.0.5. The anomalies (6 ka\_VEG-6 ka) of temperature and precipitation at  
1214 both annual and seasonal scale are presented, and all these climate variables are calculated as  
1215 the last 50-year means from two simulations.

1216